Electronic Supplementary Material (ESI) for Dalton Transactions.

Alteration of steric hindrance modulates glutathione resistance and cytotoxicity of three structurally related Ru^{II}-*p*-cymene complexes

Kallol Purkait,‡ Saptarshi Chatterjee,‡ Subhendu Karmakar and Arindam Mukherjee*

Department of Chemical Sciences, Indian Institute of Science Education and Research Kolkata, Pin 741246, India

‡ Authors contributed equally

Contents

Table S1. A few important crystal parameters for complexes **1** and **2**

	1.H_2O	**2**
Empirical formula	$C_{20}H_{25}ClF_6N_3OPRu$	$C_{22}H_{27}N_3F_6PClRu$
Formula weight	604.54	614.96
Temperature (K)	100.01(10)	99.8(4)
Wavelength(Å)	0.71073	0.71073
Crystal system,	monoclinic	triclinic
space group	$P2_1/n$	$P\bar{1}$
a (Å)	13.5912(3)	8.7779(4)
b (Å)	8.7955(2)	12.0974(6)
c (Å)	20.0691(5)	12.3892(5)
α (deg.)	90.00	113.365(4)
β (deg.)	101.465(2)	93.289(4)
γ (deg.)	90.00	97.822(4)
Volume (A^3)	2351.22(10)	1187.48(9)
Z, Calculated density (Mg/m^3)	4, 1.721	2, 1.720
F(000)	1215.0	620.0
μ/mm^{-1}	0.914	0.904
Max. and min. transmission	1.000, 0.841	1.000, 0.876
Goodness-of-fit on F^2	1.020	1.052
Final R indices [I>2sigma(I)]	$^aR_1$ = 0.0399, $^bwR_2$ = 0.0979	$^aR_1$ = 0.0282, $^bwR_2$ = 0.0624
R indices (all data)	$^aR_1$ = 0.0463, $^bwR_2$ = 0.1032	$^aR_1$ = 0.0314, $^bwR_2$ = 0.0652

$^aR_1 = \Sigma||F_o| - |F_c||/\Sigma|F_o|$. $^bwR_2 = [\Sigma[w(F_o^2 - F_c^2)^2]/\Sigma w(F_o^2)^2]^{1/2}$

Table S2. Selected bond lengths (Å) and angles (°) for complex **1** and **2**.

1.H_2O				**2**			
Ru1-Cl1	2.416(9)	N2-Ru1-N1	76.41(11)	Ru1-Cl1	2.410 (7)	N1-Ru1-N3	76.27(8)
Ru1-N1	2.114(3)	N1-Ru1-Cl1	87.19(8)	Ru1-N1	2.077(2)	N1-Ru1-Cl1	83.66(6)
Ru1-N2	2.080(3)	N2-Ru1-Cl1	84.96(8)	Ru1-N3	2.133(2)	N3-Ru1-Cl1	88.83(6)
Ru1-C11	2.195(3)	N2-Ru1-C11	96.17(11)	Ru1-C13	2.245(2)	N1-Ru1-C13	160.95(9)
Ru1-C12	2.161	N2-Ru1-C12	122.85(11)	Ru1-C14	2.216(2)	N1-Ru1-C14	155.10(9)
Ru1-C13	2.198(3)	N2-Ru1-C13	159.96(11)	Ru1-C15	2.192(3)	N1-Ru1-C15	118.06(9)
Ru1-C14	2.240(4)	N2-Ru1-C14	155.45(11)	Ru1-C16	2.205(3)	N1-Ru1-C16	93.62(9)
Ru1-C15	2.185(4)	N2-Ru1-C15	119.43(11)	Ru1-C17	2.184(3)	N1-Ru1-C17	96.53(9)
Ru1-C16	2.175(3)	N2-Ru1-C16	95.24(11)	Ru1-C18	2.179(3)	N1-Ru1-C18	122.94(9)

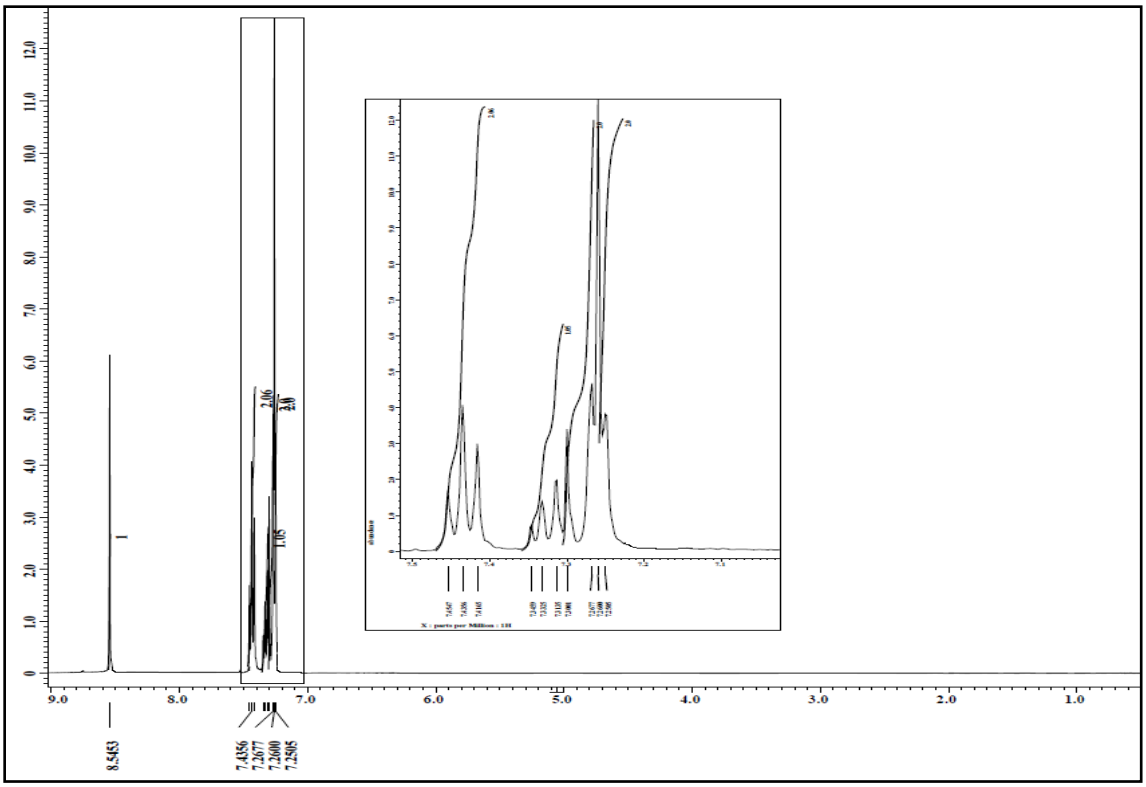

Fig. S1 ^{1}H NMR spectrum of complex **L1** in $CDCl_3$.Inset: the aromatic region.

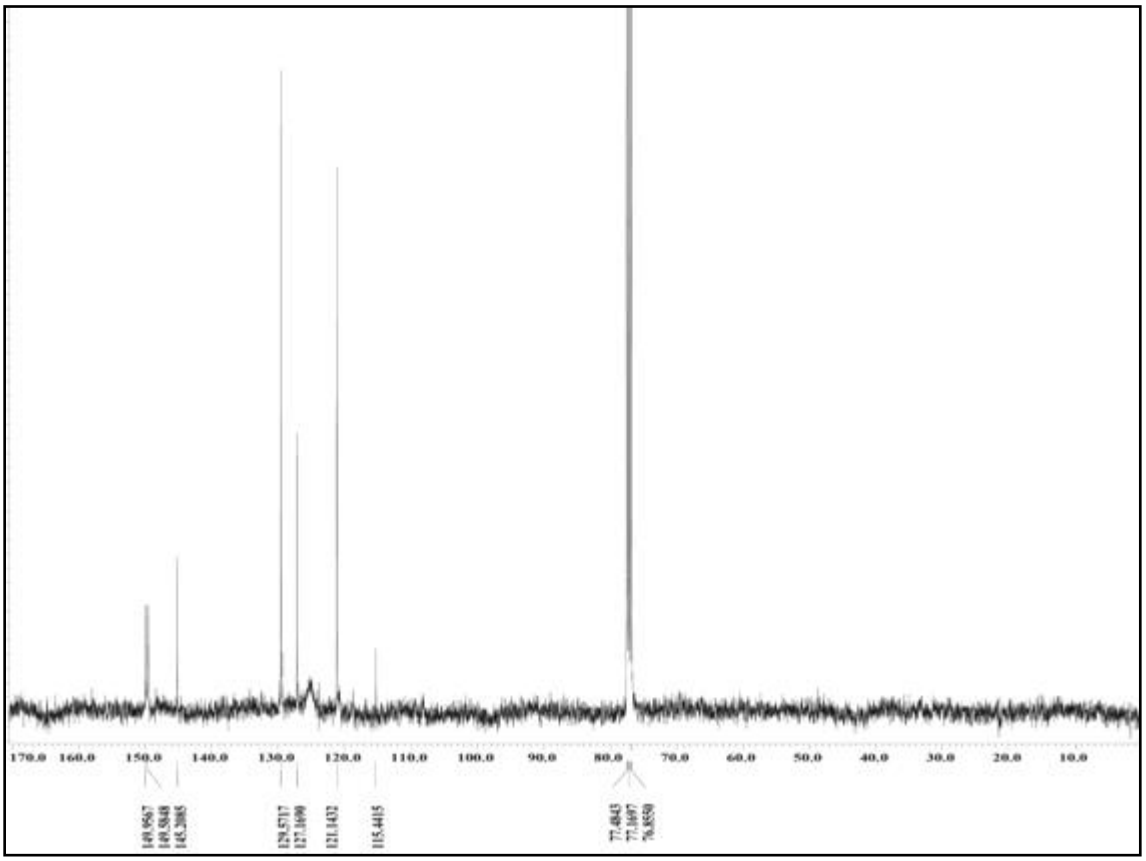

Fig. S2 ^{13}C NMR of **L1** in $CDCl_3$.

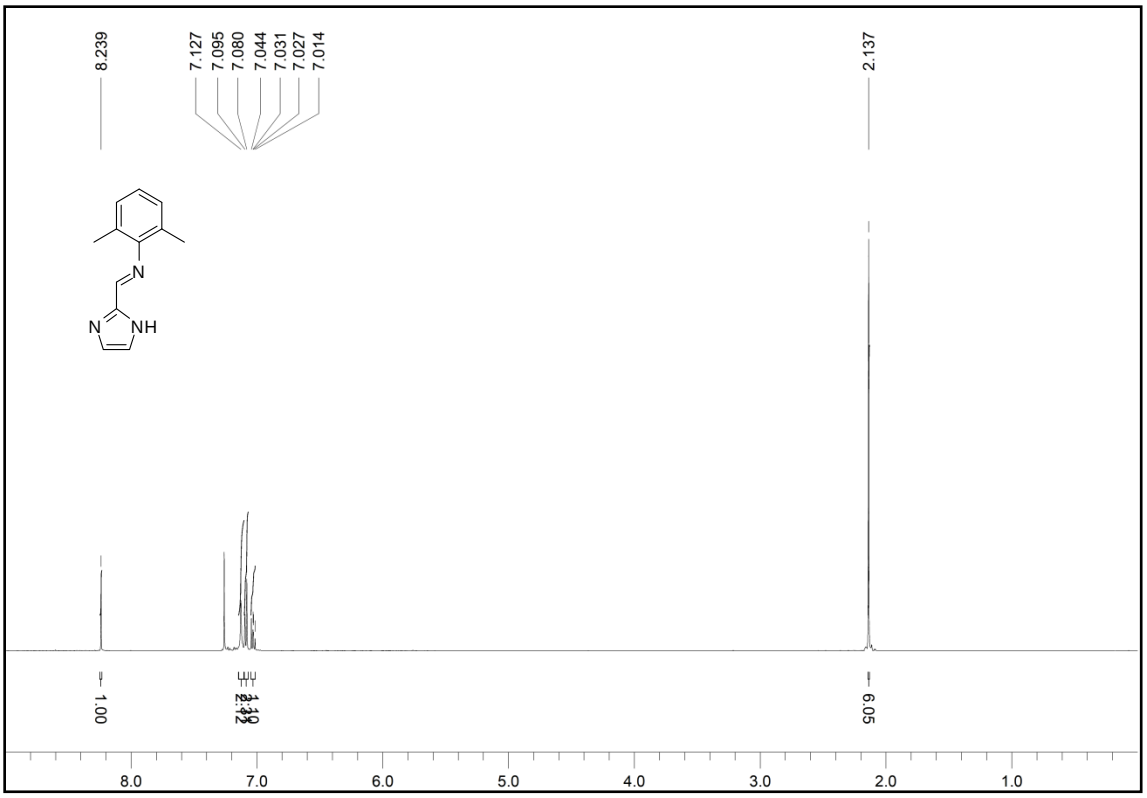

Fig. S3 ^{1}H NMR spectrum of complex **L2** in $CDCl_3$.

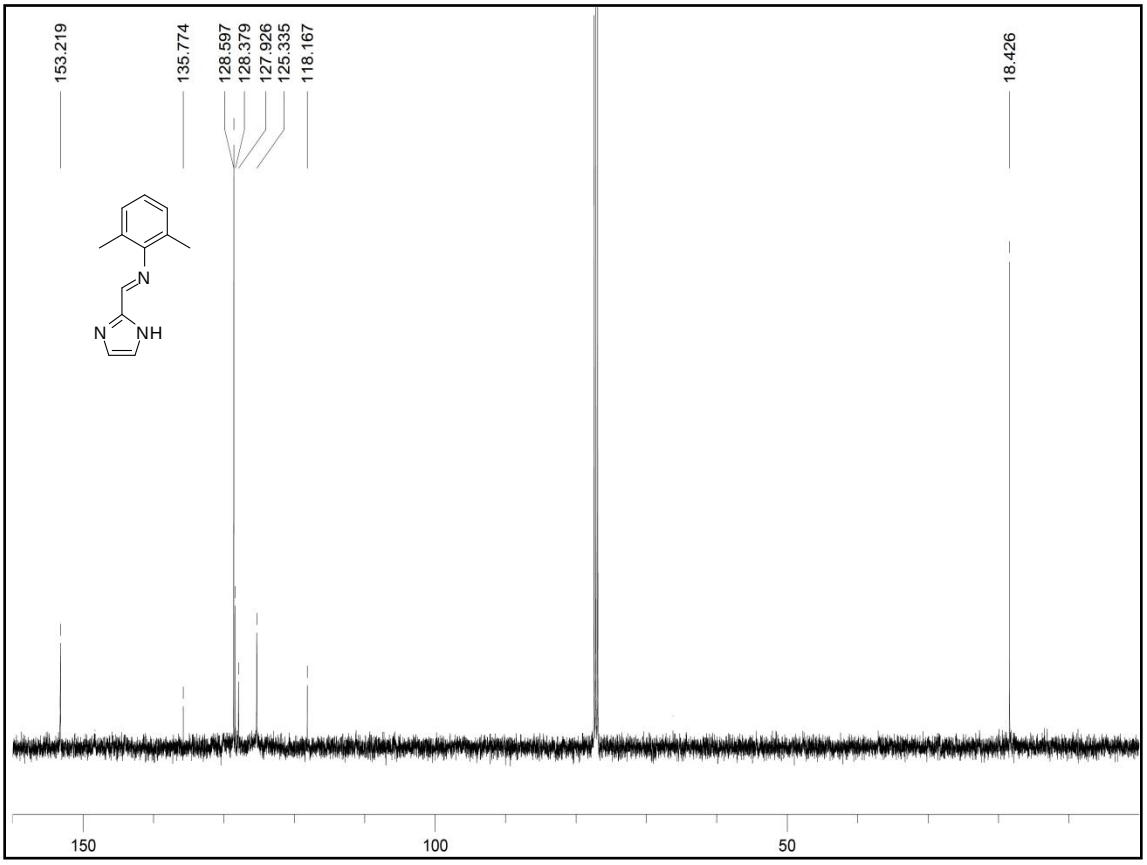

Fig. S4 ^{13}C NMR of **L2** in $CDCl_3$.

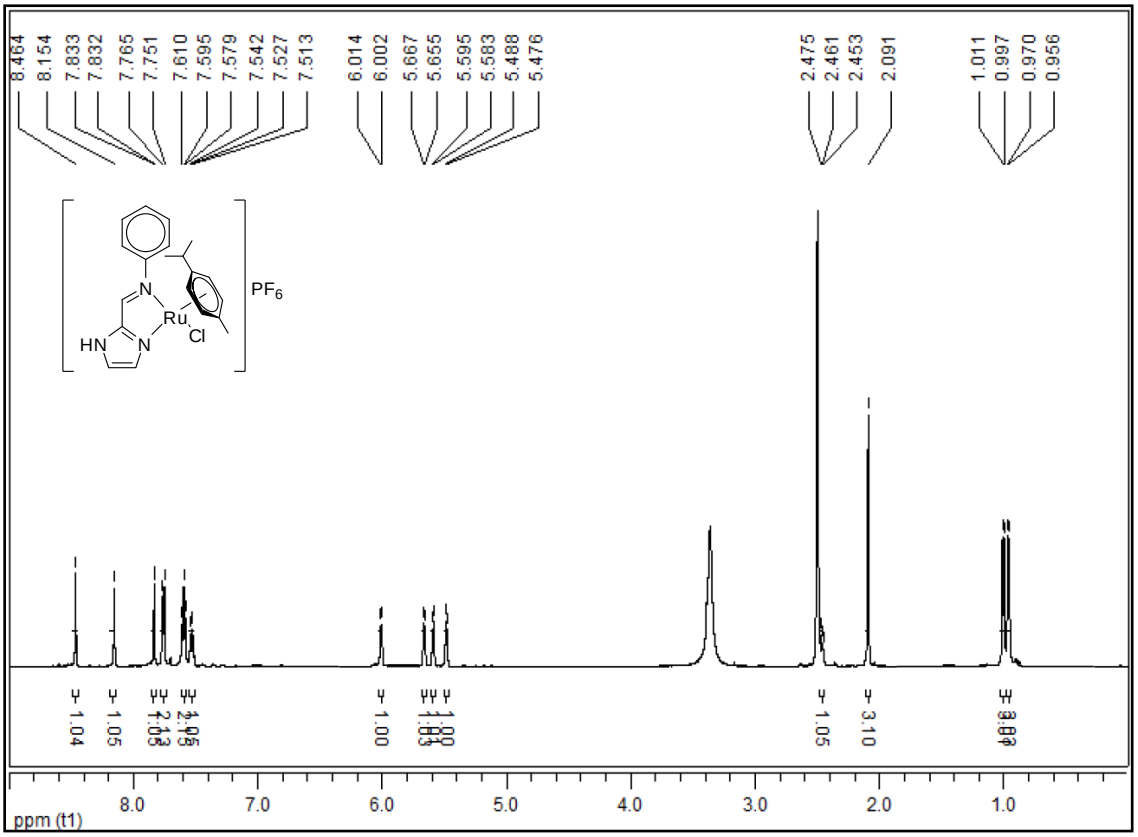

Fig. S5 ^{1}H NMR spectrum of complex **1** in DMSO-d_6

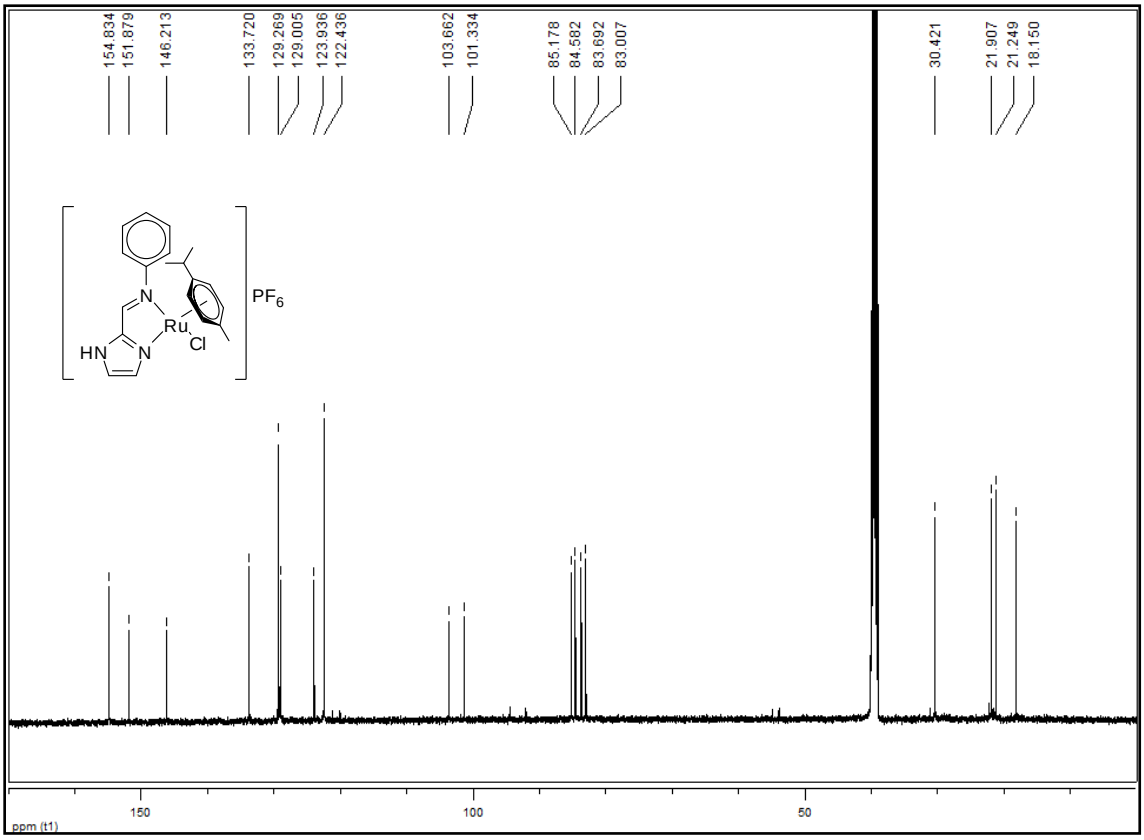

Fig. S6 ^{13}C NMR of **1** in DMSO-d_6

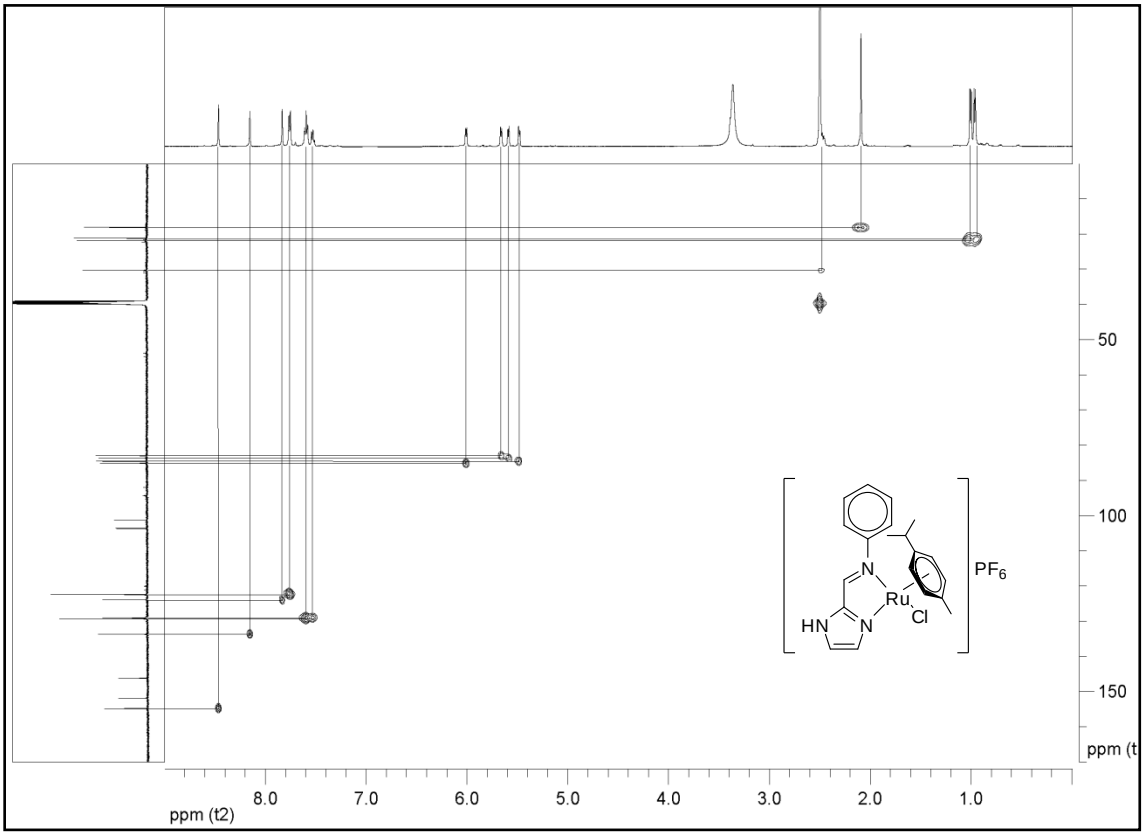

Fig. S7 HMQC of **1** in DMSO-d_6

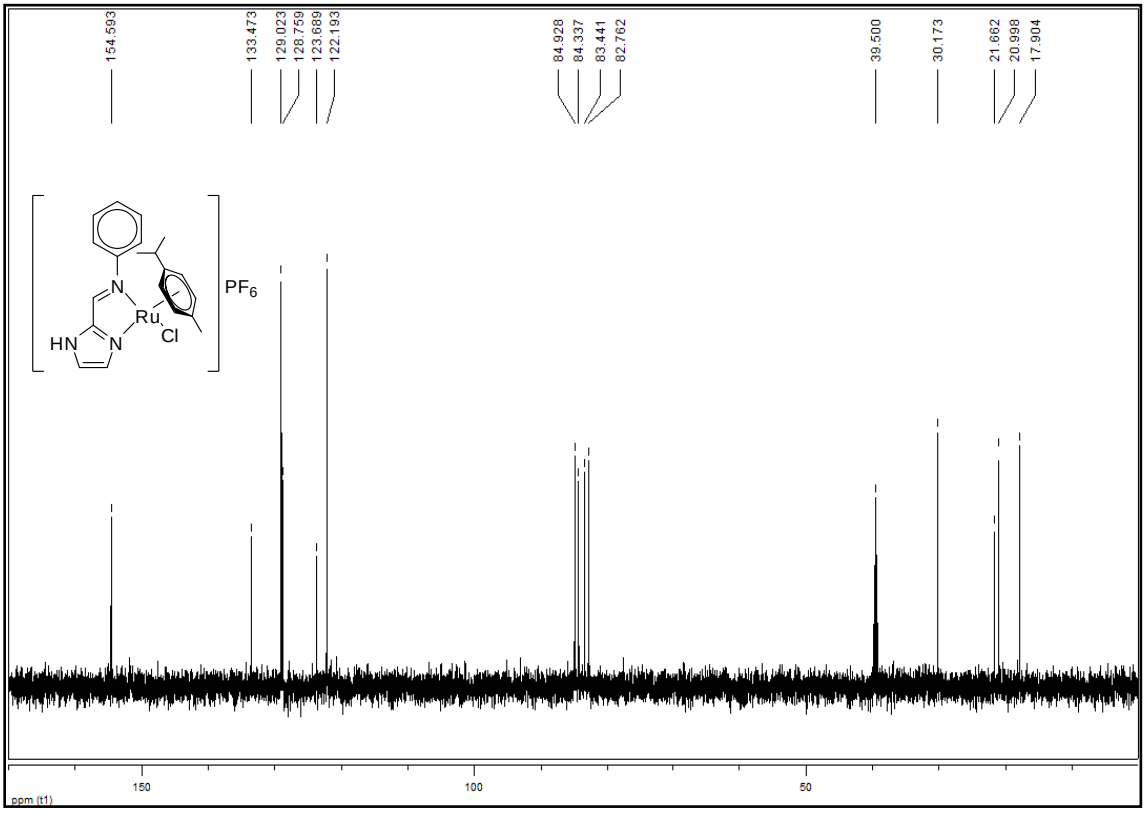

Fig. S8 DEPT 135 of **1** in DMSO-d_6

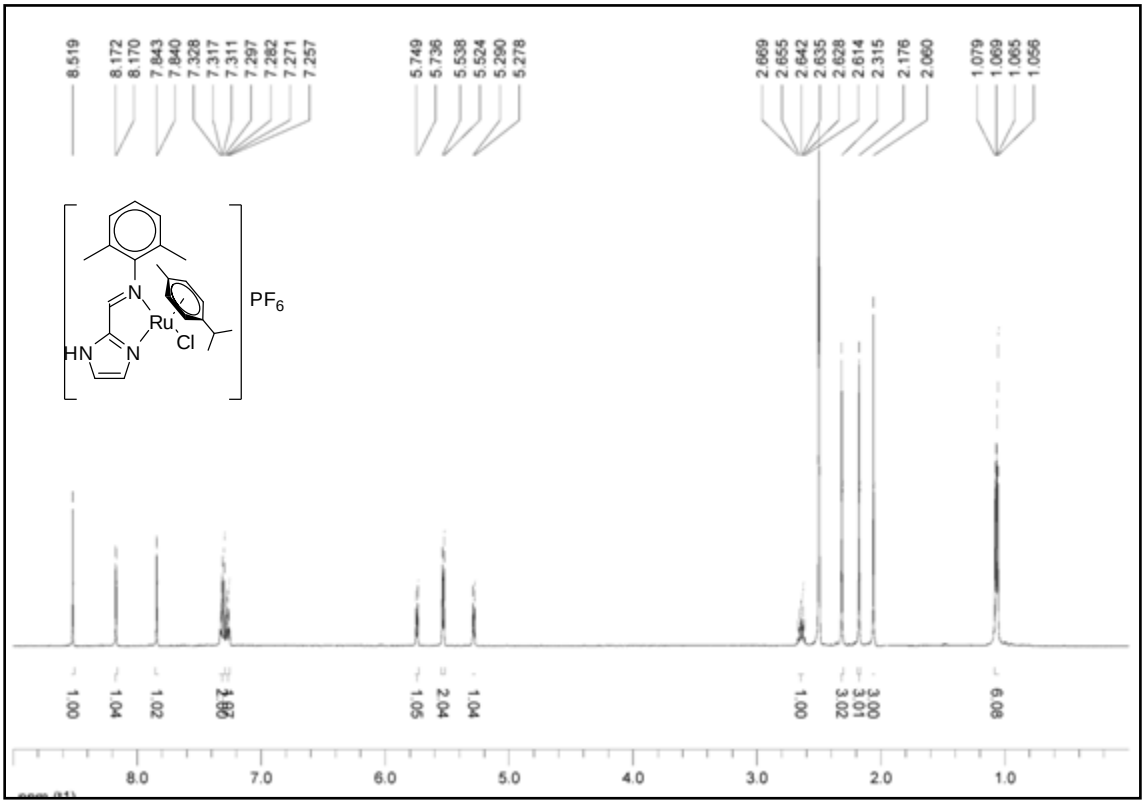

Fig. S9 ^{1}H NMR spectrum of complex **2** in DMSO-d_6

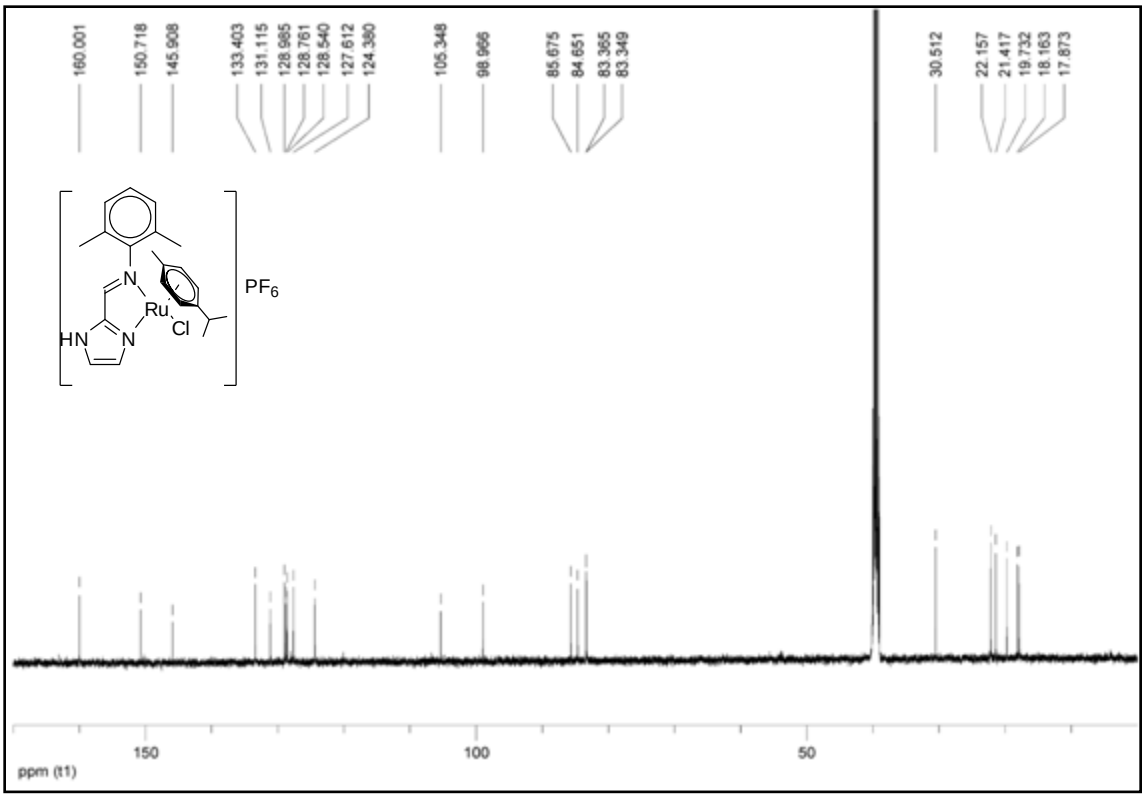

Fig. S10 ^{13}C NMR of **2** in DMSO-d_6

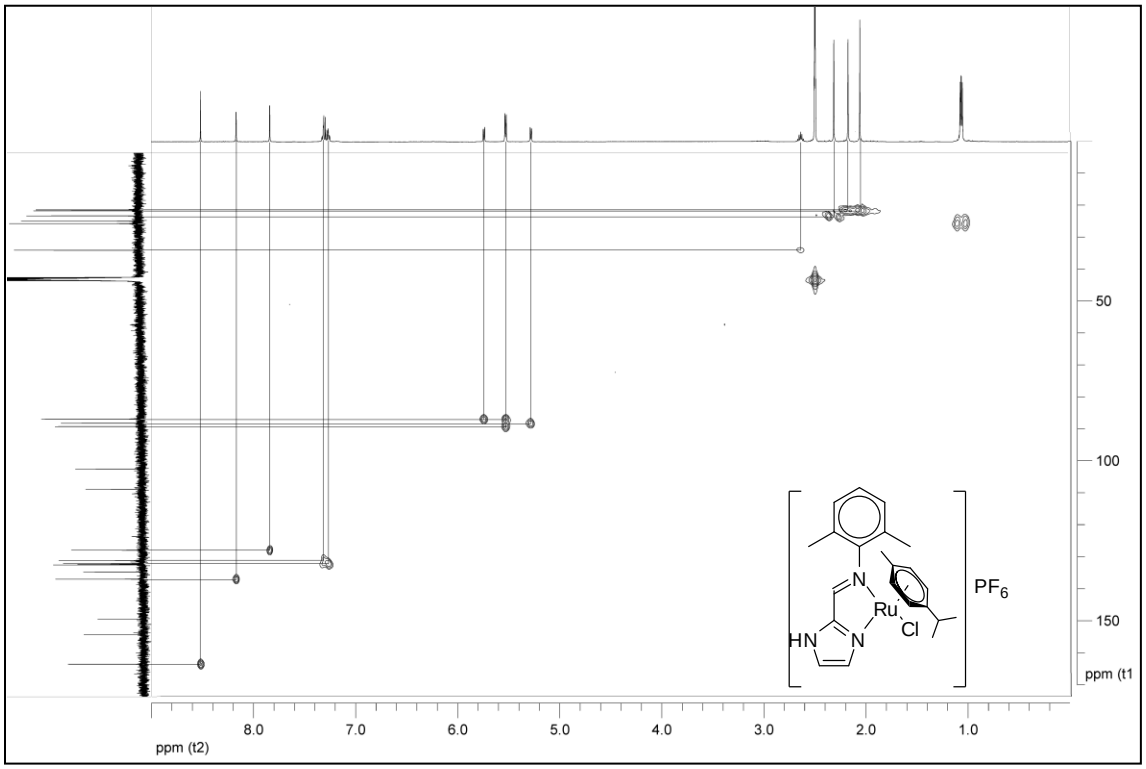

Fig. S11 HMQC of **2** in DMSO-d_6

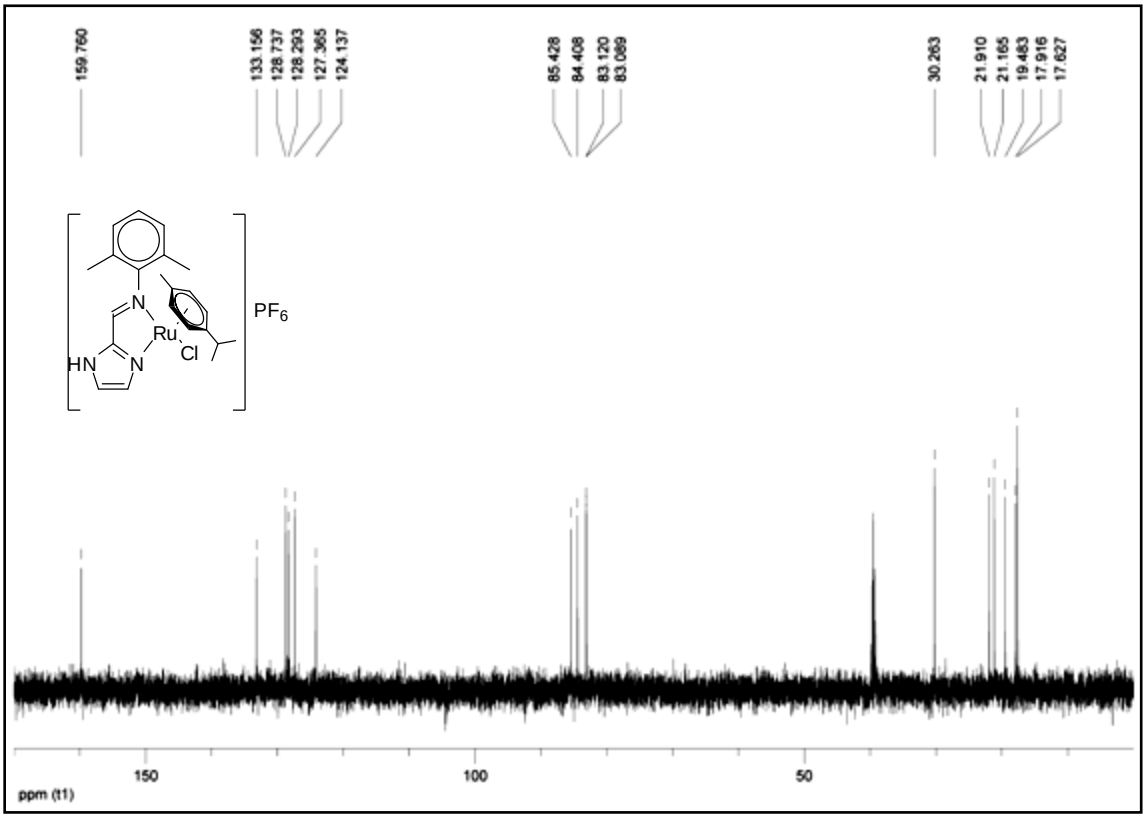

Fig. S12 DEPT 135 of **2** in DMSO-d_6

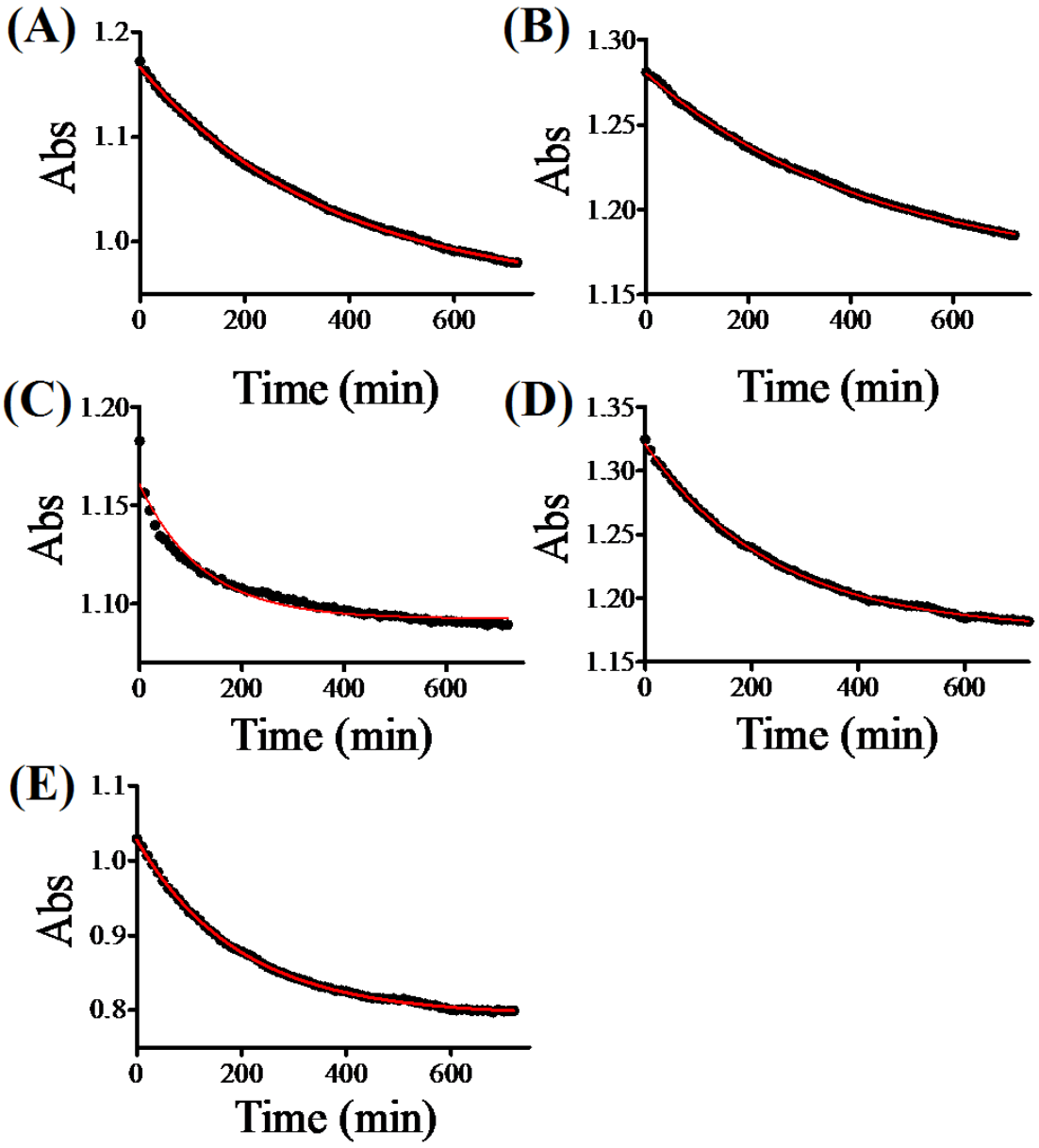

Fig. S13 Hydrolysis of **1** measured by UV-Visible spectroscopy. 1% methanol-aqueous phosphate buffer solution at pH 7.4 in presence of – (A) 4 mM and (B) 40 mM NaCl; at pH 6.7 in presence of – (C) 4 mM and (D) 40 mM NaCl. (E) in 1% methanol-water mixture. The plots provided are for one independent experiment out of the three independent experiments performed and the fitting is performed using monoexponential decay function.

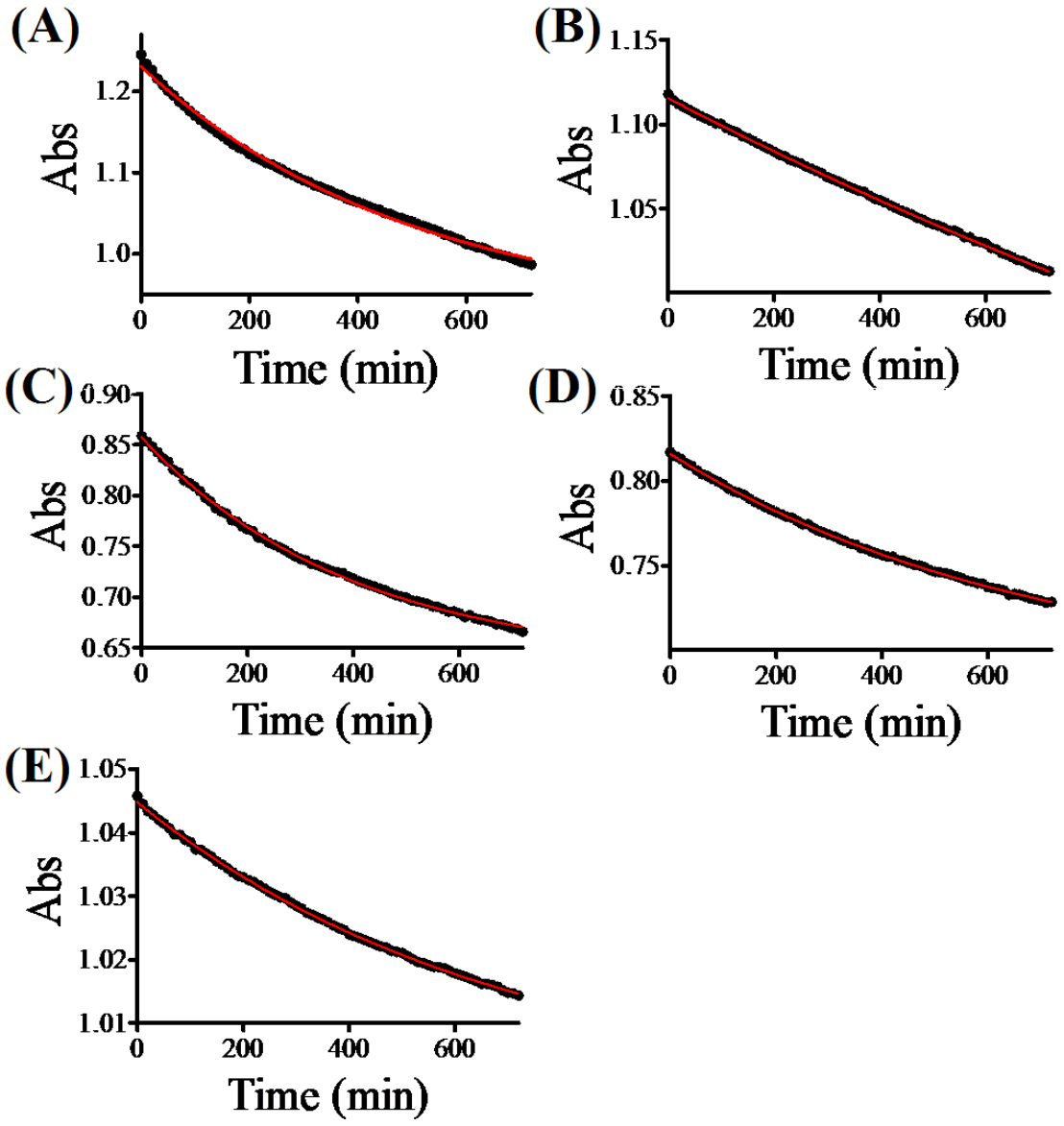

Fig. S14 Hydrolysis of **2** using UV-Visible spectroscopy fitted using monoexponential decay function. 1% methanol-aqueous phosphate buffer solution at pH 7.4 using – (A) 4 mM and (B) 40 mM NaCl; at pH 6.7 using (C) 4 mM and (D) 40 mM NaCl. (E) in 1% methanol-water mixture. The plots provided are for one independent experiment out of the three independent experiments performed.

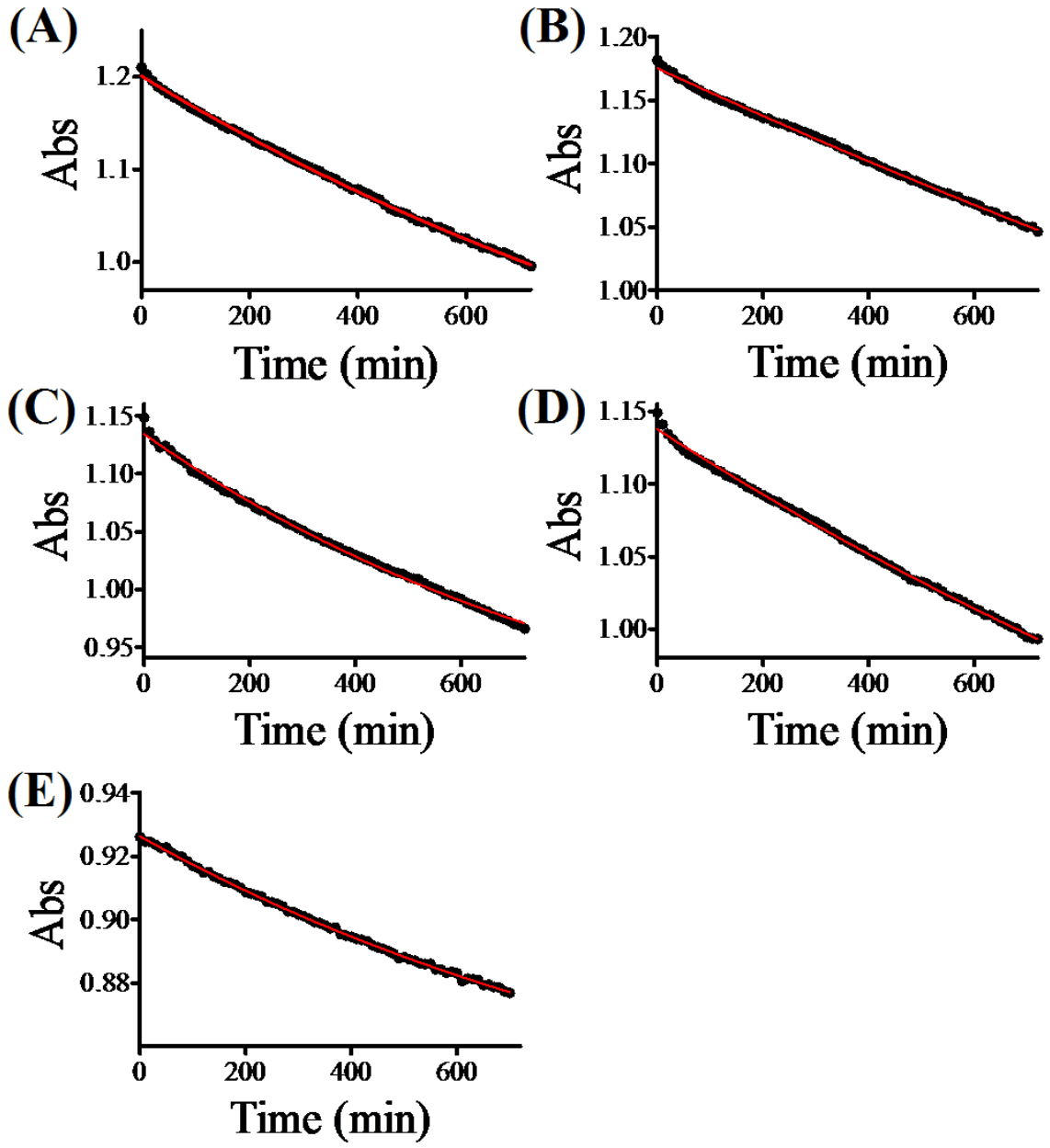

Fig. S15 Hydrolysis of **3** measured by UV-Visible spectroscopy. 1% methanol-aqueous phosphate buffer solution at pH 7.4 in presence of – (A) 4 mM and (B) 40 mM NaCl; at pH 6.7 in presence of – (C) 4 mM and (D) 40 mM NaCl. (E) in 1% methanol-water mixture. The plots provided are for one independent experiment out of the three independent experiments performed and the fitting is performed using monoexponential decay function.

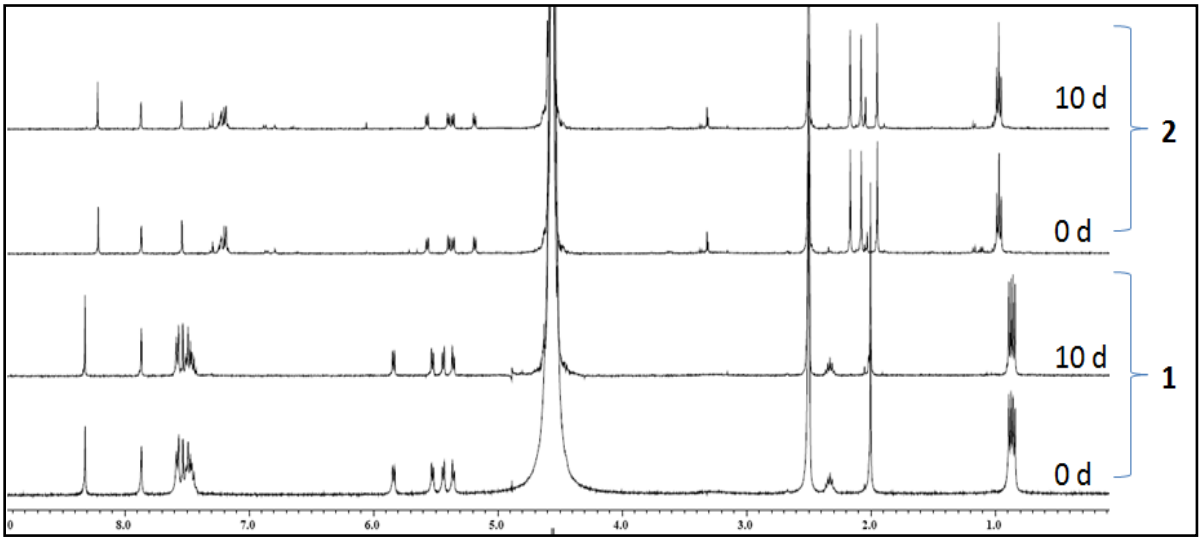

Fig. S16 Time dependent ^{1}H NMR spectra of complex **1-2** in 110 mM NaCl solution using 30% DMSO-d_6 in D_2O at 25°C. *t* = 0 d, stands for the spectra recorded immediately after dissolving of respective complex.

Table S3. Rate of hydrolysis for complexes **1**, **2** and **3** measured by UV-Vis spectroscopy.

pH	Chloride conc. (mM)	**1**	**2**	**3**
		$k \pm$ S.D.[a] $\times 10^{-1}$ (h^{-1})	$k \pm$ S.D.[a] $\times 10^{-2}$ (h^{-1})	$k \pm$ S.D.[a] $\times 10^{-2}$ (h^{-1})
7.4	4	2.56 ± 0.6	12.2 ± 0.3	3.90 ± 0.1
	40	2.02 ± 0.9	3.12 ± 0.2	1.40 ± 0.1
6.7	4	6.19 ± 1.8	15.9 ± 1.1	8.60 ± 0.3
	40	2.72 ± 0.2	7.25 ± 2.1	2.92 ± 0.2
Water	-	3.46 ± 0.4	9.17 ± 0.5	6.06 ± 1.29
[a] Standard deviation				

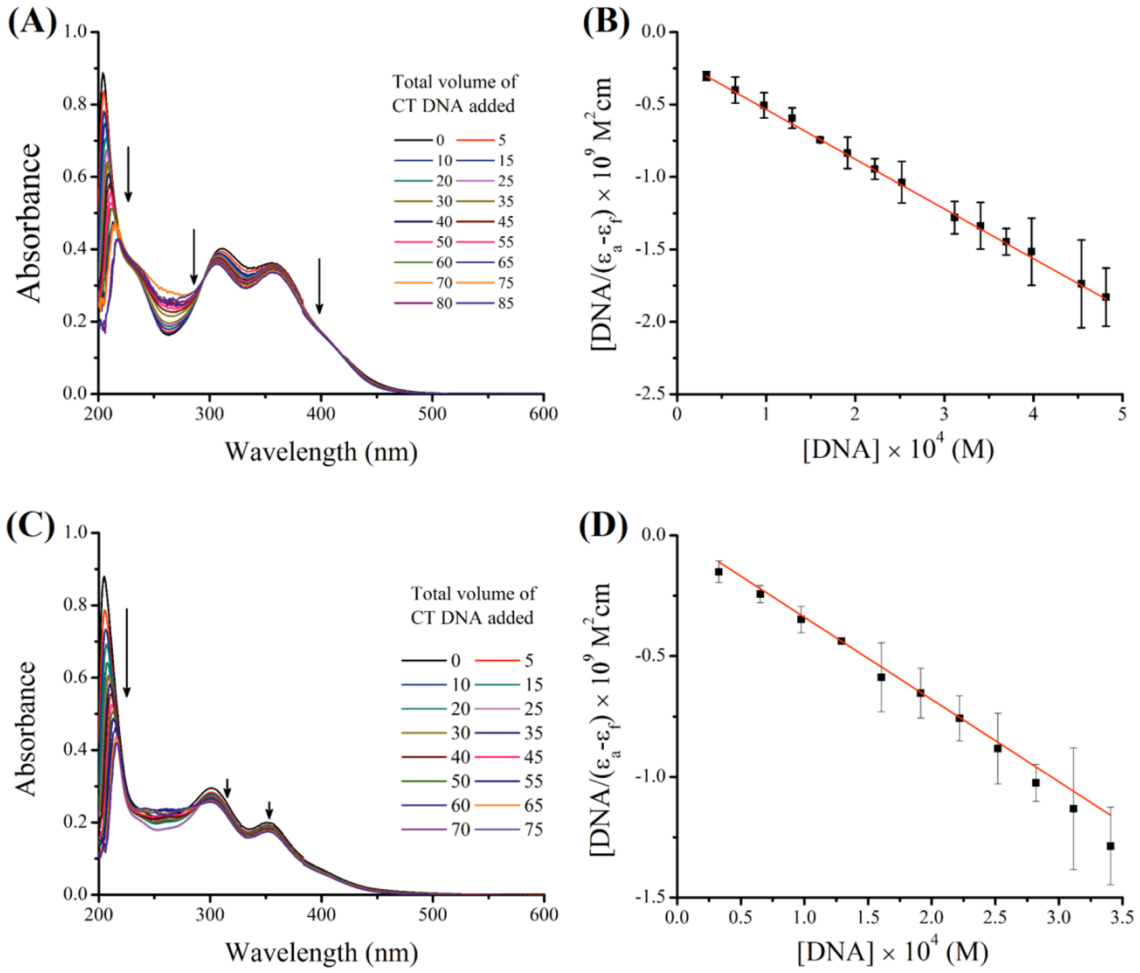

Fig. S17 A) and C) Absorption spectral change upon addition of CT DNA solution to a fresh solution of **1** and **2** respectively in Tris-NaCl/MeCN (99:1 *v/v*) at pH 7.4 (T = 25 °C). The plots provided are of one independent experiment out of the three independent experiments performed. B) and D) The plot of [DNA]/ (ε_a - ε_f) vs [DNA] for complex **1** and **2** respectively to calculate apparent binding constant (K_b) using the mean of three independent experiments along with the standard deviation.

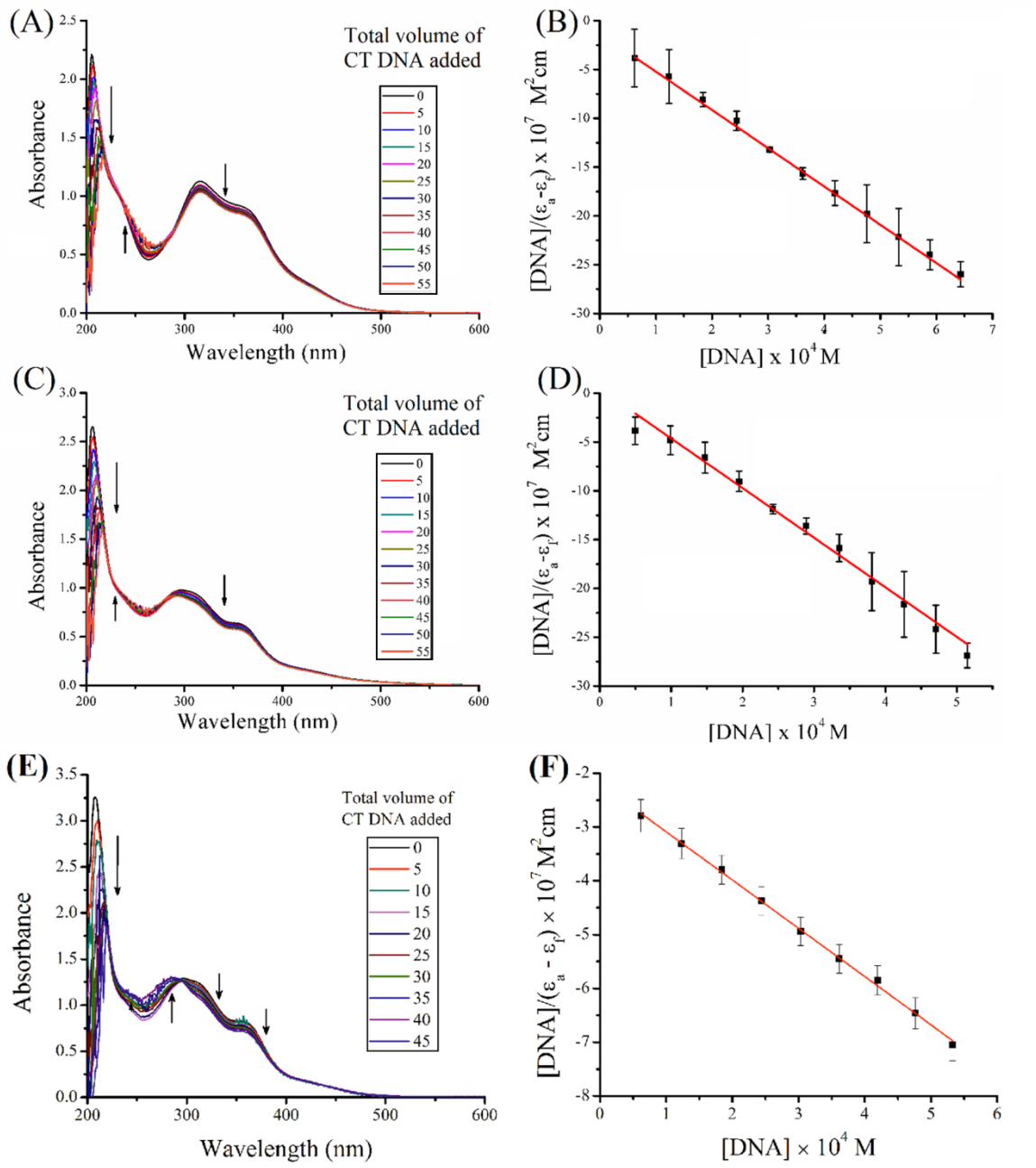

Fig. S18 A), C) and E) Absorption spectral change upon addition of CT DNA solution to 12 h hydrolysed solution of **1, 2** and **3** respectively in Tris-NaCl/MeCN (99:1 *v/v*) at pH 7.4 (T= 25 °C). B), D) and F) The plot of [DNA]/ (ε_a - ε_f) vs [DNA] for complex **1**, **2** and **3** respectively to calculate apparent binding constant (K_b). The data fitting plots (B, D and F) are done with the mean of three independent experiments along with the standard deviation.

Table S4. CT DNA binding constant for complex **1-3**.

Complex	Binding constant (K_b M^{-1})	
	0 h of hydrolysis prior to binding	12 h of hydrolysis prior to binding
1	$3.03\ (0.6) \times 10^4$	$3.04\ (0.1) \times 10^4$
2	$1.11\ (0.1) \times 10^5$	$1.11\ (0.3) \times 10^5$
3	[a]$2.30\ (3) \times 10^3$	$4.11\ (2.9) \times 10^3$

All the results are the mean of three experiments. [a]data was obtained from ref. 1. The values within the bracket indicate standard deviation.

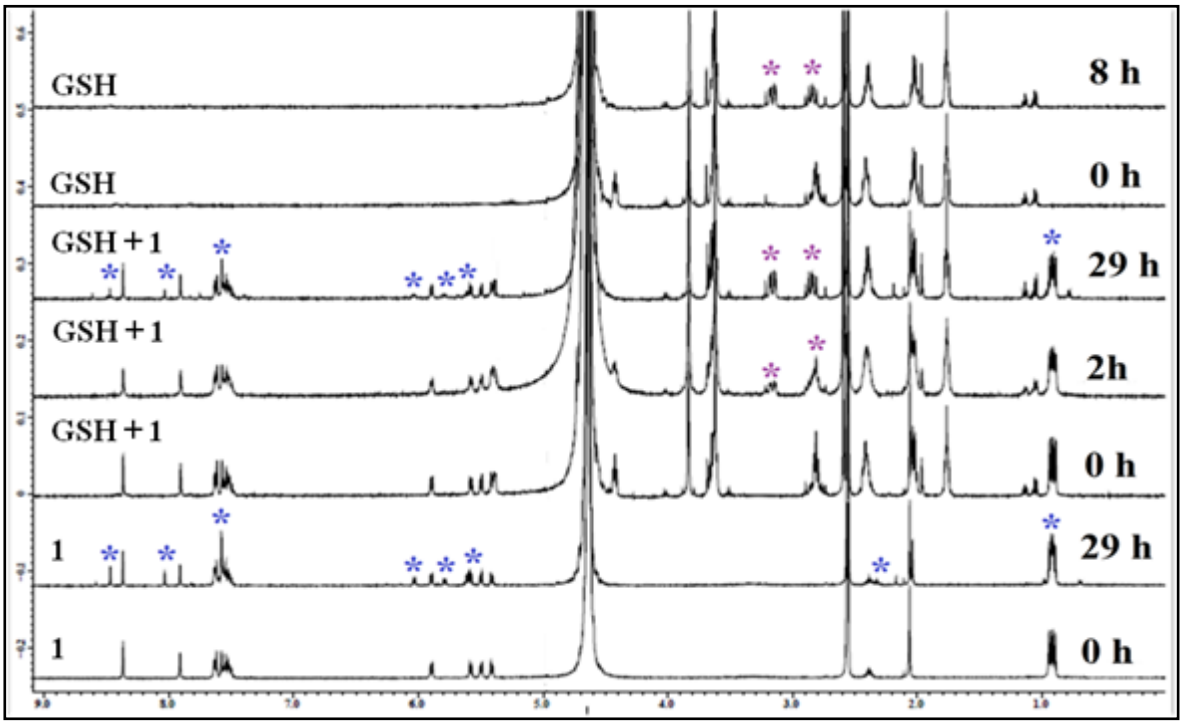

Fig. S19 Stack plot of ^{1}H NMR spectra of reduced L-glutathione at 0 h and 8 h (first two above), complex **1** at 0 h and 29 h (last two below), complex **1** and reduced L-glutathione (middle three) in 30% DMSO-d_6/D_2O mixture, recorded at different interval of time at 25°C. t = 0 h, stands for the spectra recorded immediately after dissolving reduced L-glutathione and complex **1**. *stands for hydrolysis product, *stands for GSH auto-oxidation product.

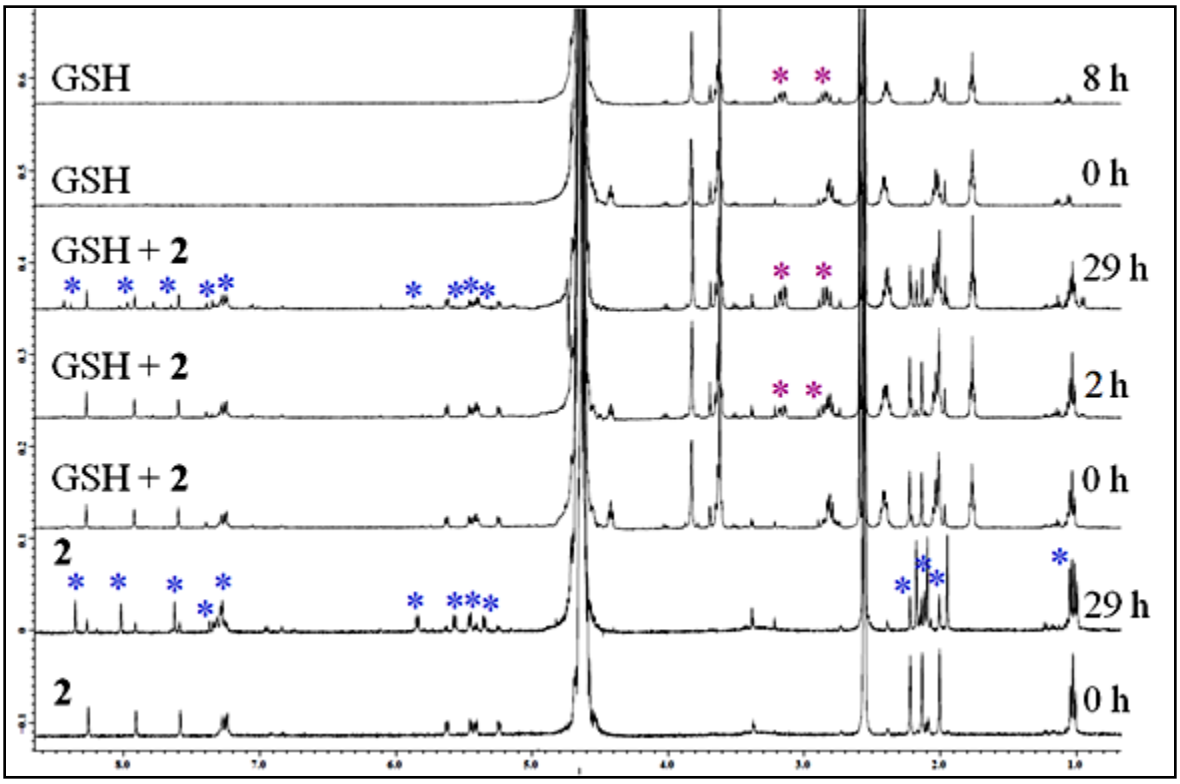

Fig. S20 Stack plot of ^{1}H NMR spectra of reduced L-glutathione at 0 h and 8 h (first two above), complex **2** at 0 h and 29 h (last two below), complex **2** and reduced L-glutathione (middle three) in 30% DMSO-d_6/D_2O mixture, recorded at different interval of time at 25°C. t = 0 h, stands for the spectra recorded immediately after dissolving reduced L-glutathione and complex **2**. *stands for hydrolysis product, *stands for GSH auto-oxidation product.

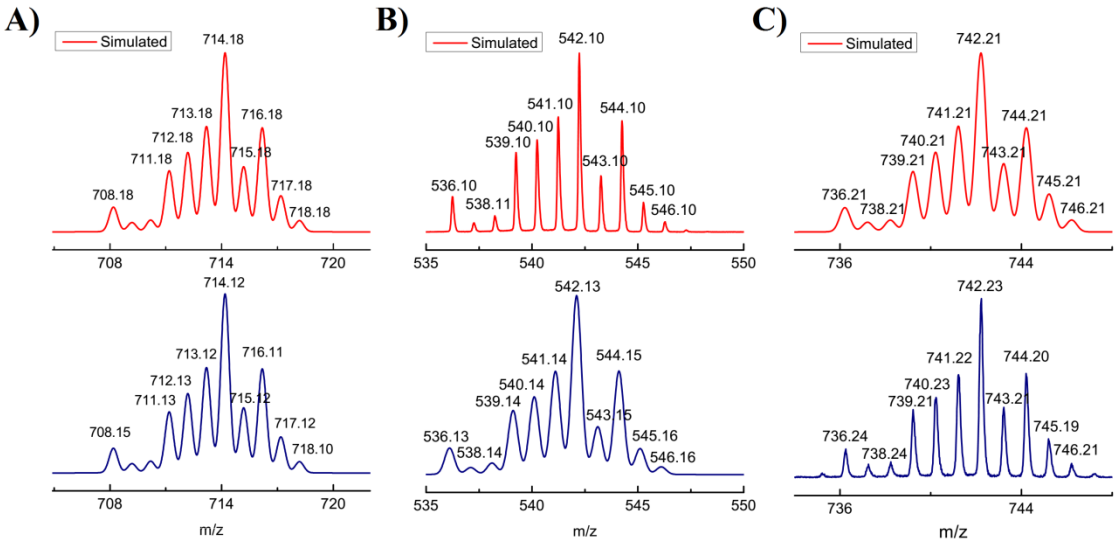

Fig. S21 ESI mass spectra of GSH bound species with A) complex **1**, B) and C) complex **2**. Red lines are for simulated spectra, Blue lines are for observed spectra.

A)

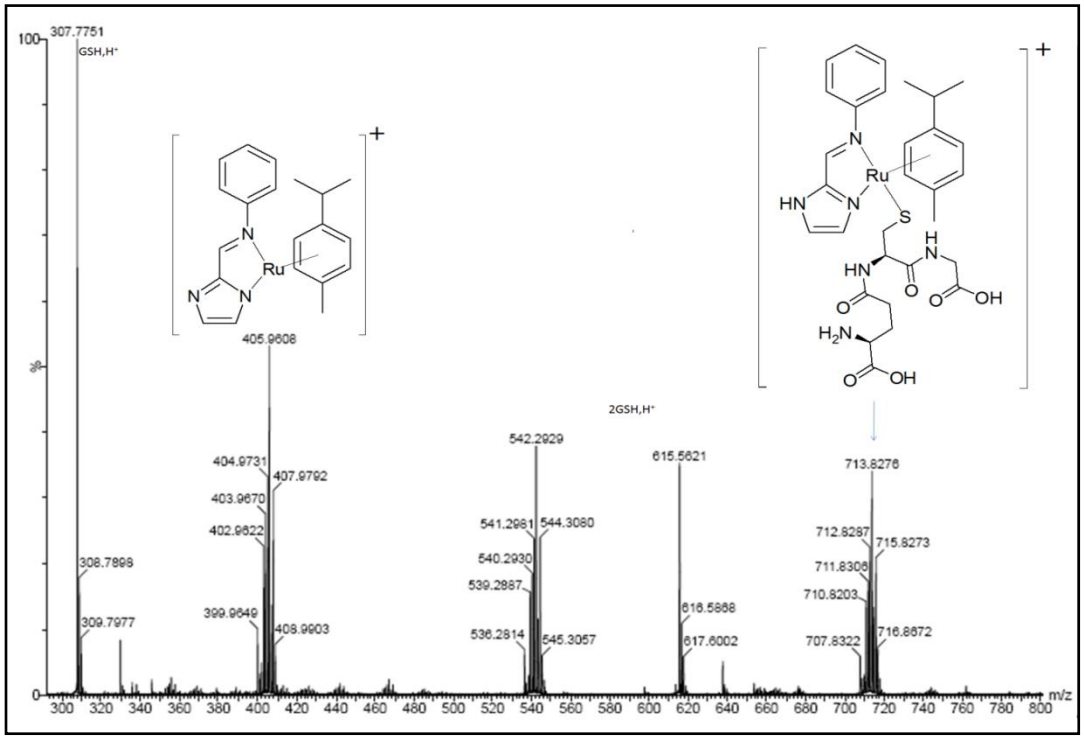

B)

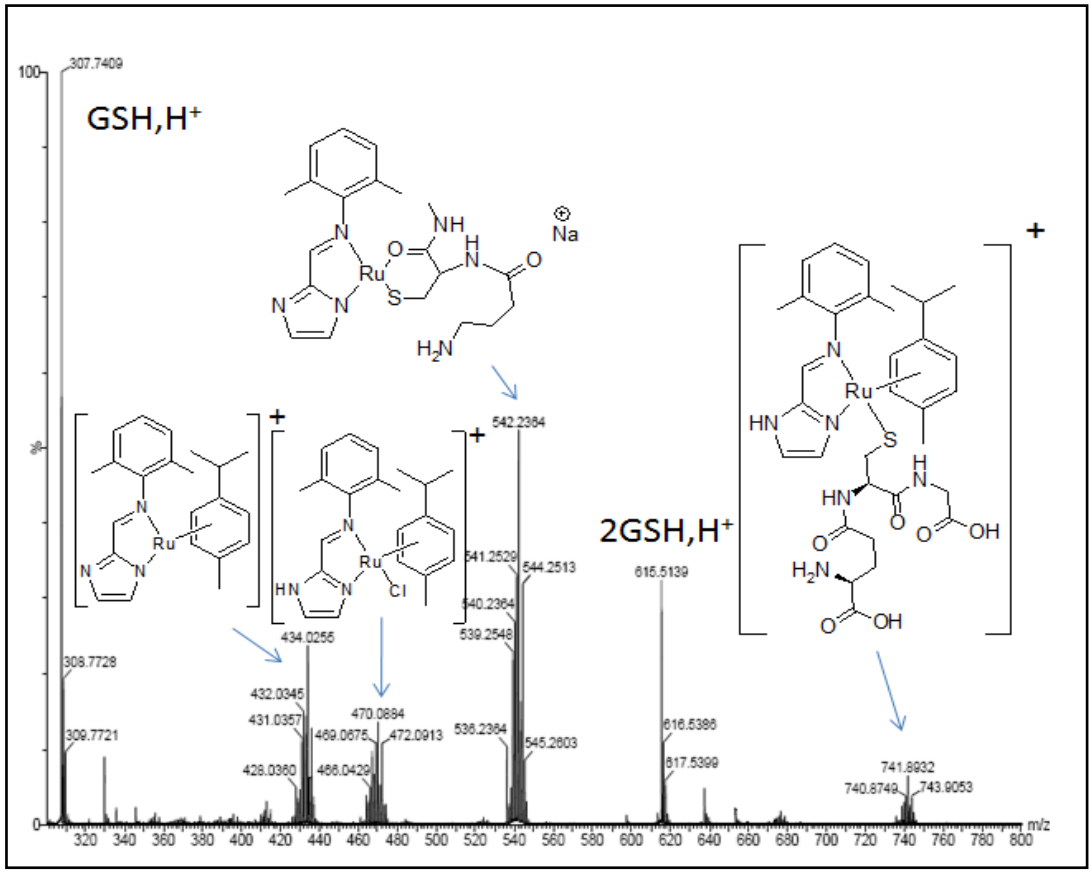

Fig. S22 ESI Mass spectra of GSH binding adduct with A) complex **1** and B) complex **2**, after incubation for 30 min of complex with 25 equivalent of GSH.

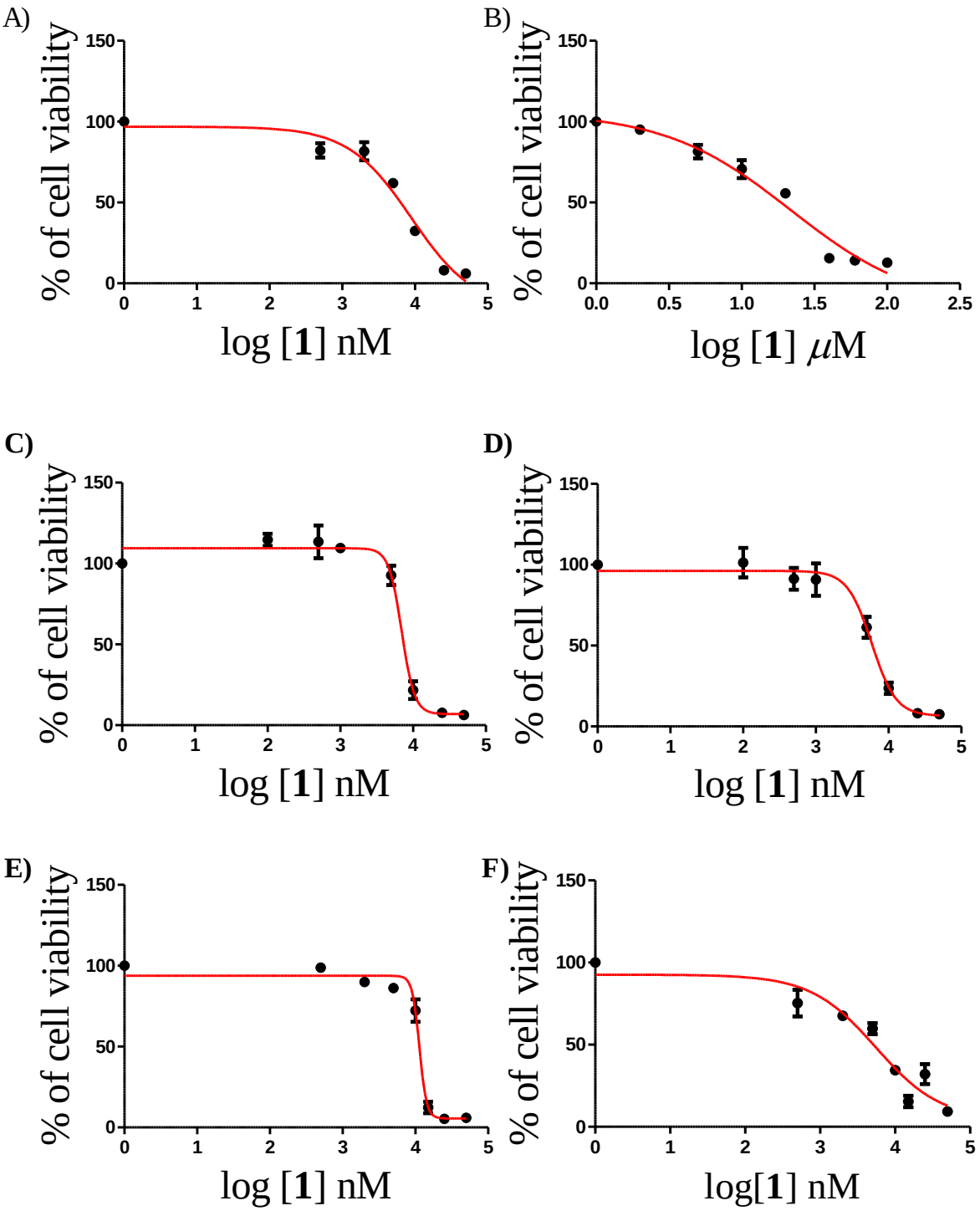

Fig. S23 Plots of cell viability (%) vs. log of concentration for **1** A) MCF-7, B) A549, C) MIA PaCa-2, D) HepG2, E) NIH 3T3 and F) Human primary Foreskin fibroblast cell lines after incubation for 48 h, under normoxic condition through MTT assay. The plots provided are for one independent experiment out of the three independent experiments performed with each concentration.

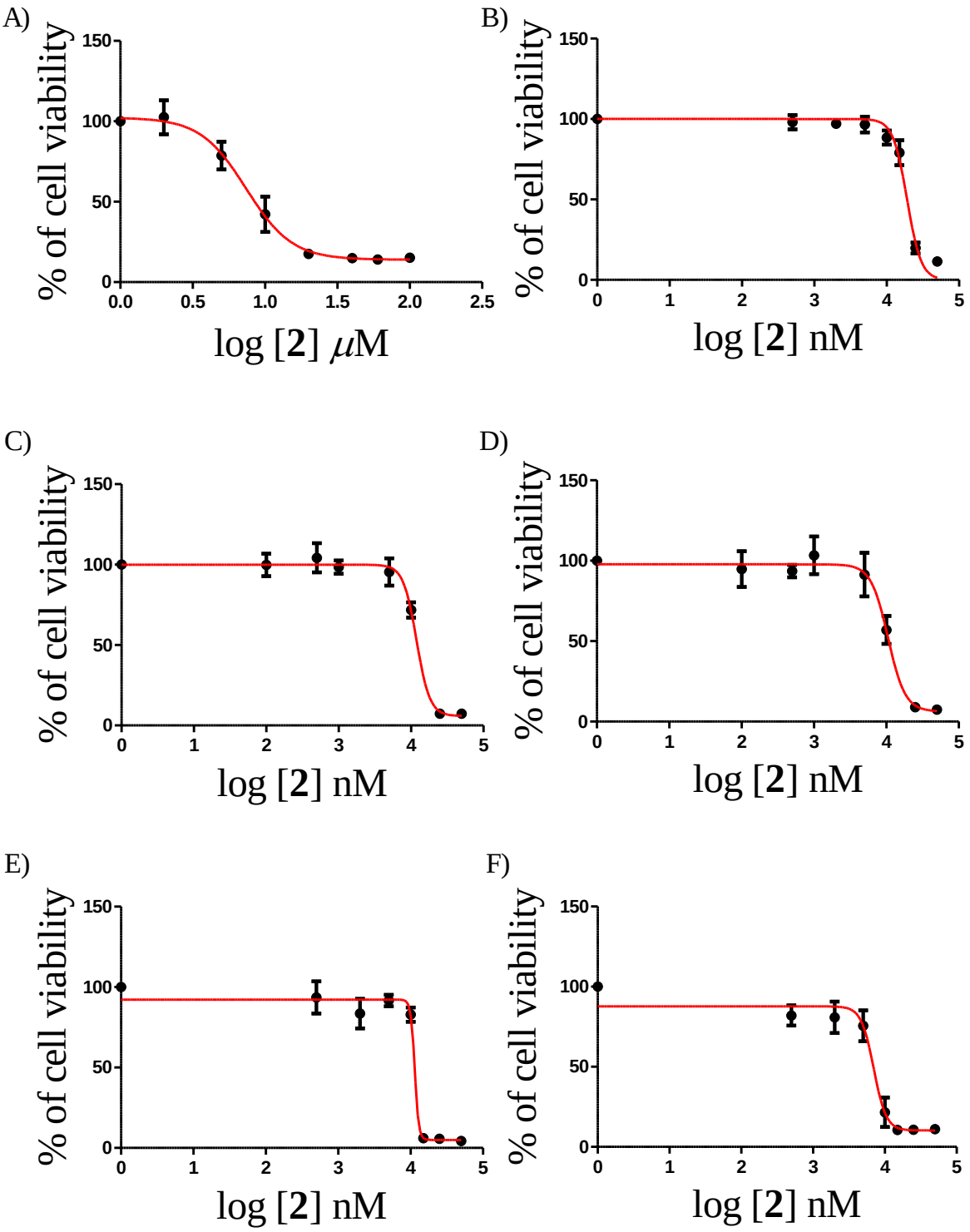

Fig. S24 Plots of cell viability (%) vs. log of concentration for **2** A) MCF-7, B) A549, C) MIAPaCa-2, D) HepG2, E) NIH 3T3 and F) Human primary Foreskin fibroblast cell lines after incubation for 48 h, determined from MTT assays under normoxic condition. The plots provided are for one independent experiment out of the three independent experiments performed with each concentration.

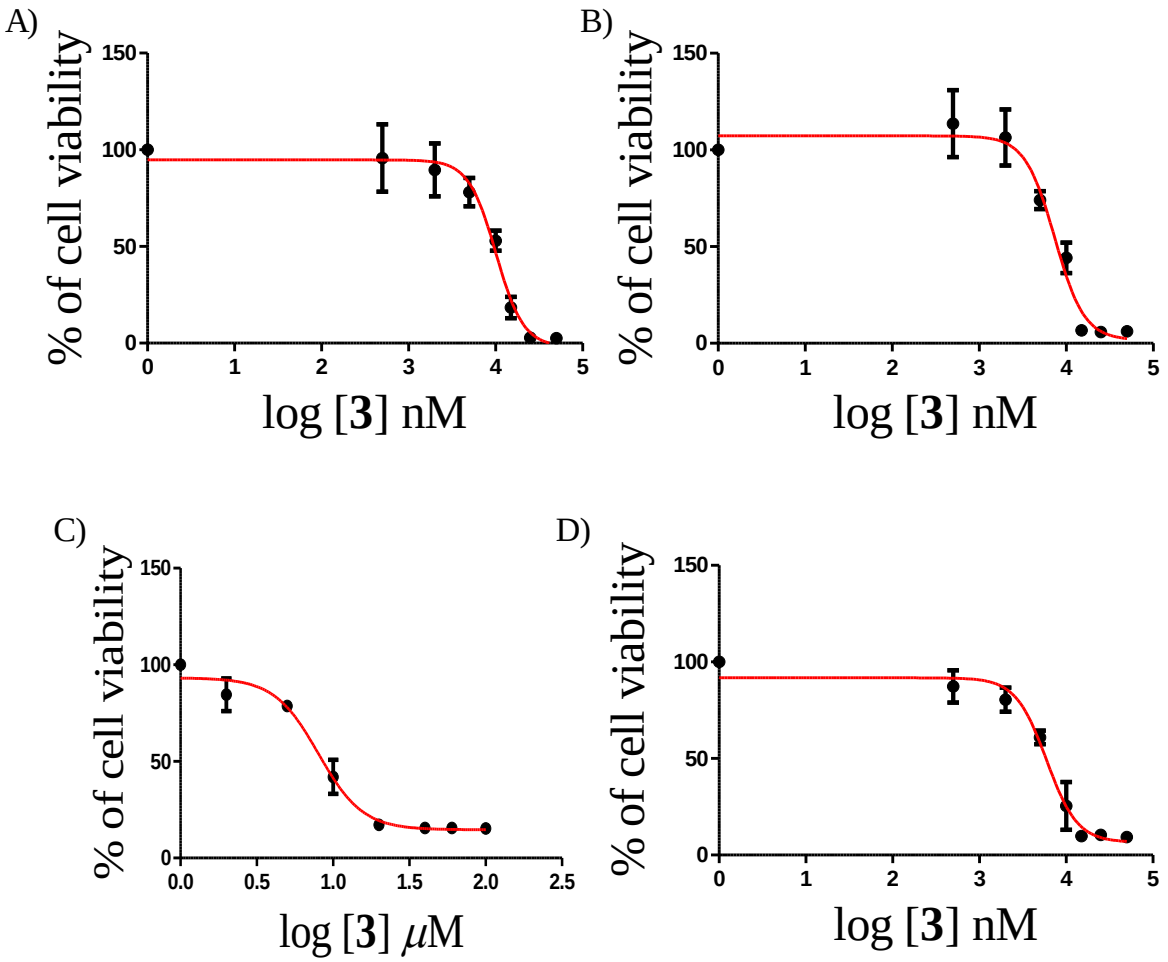

Fig. S25 Plots of cell viability (%) vs. log of concentration for **3** A) MIA PaCa-2, B) HepG2, C) NIH 3T3 and D) Human primary Foreskin fibroblast cell lines after incubation for 48 h, determined from MTT assays under normoxic condition. The plots provided are for one independent experiment out of the three independent experiments performed with each concentration.

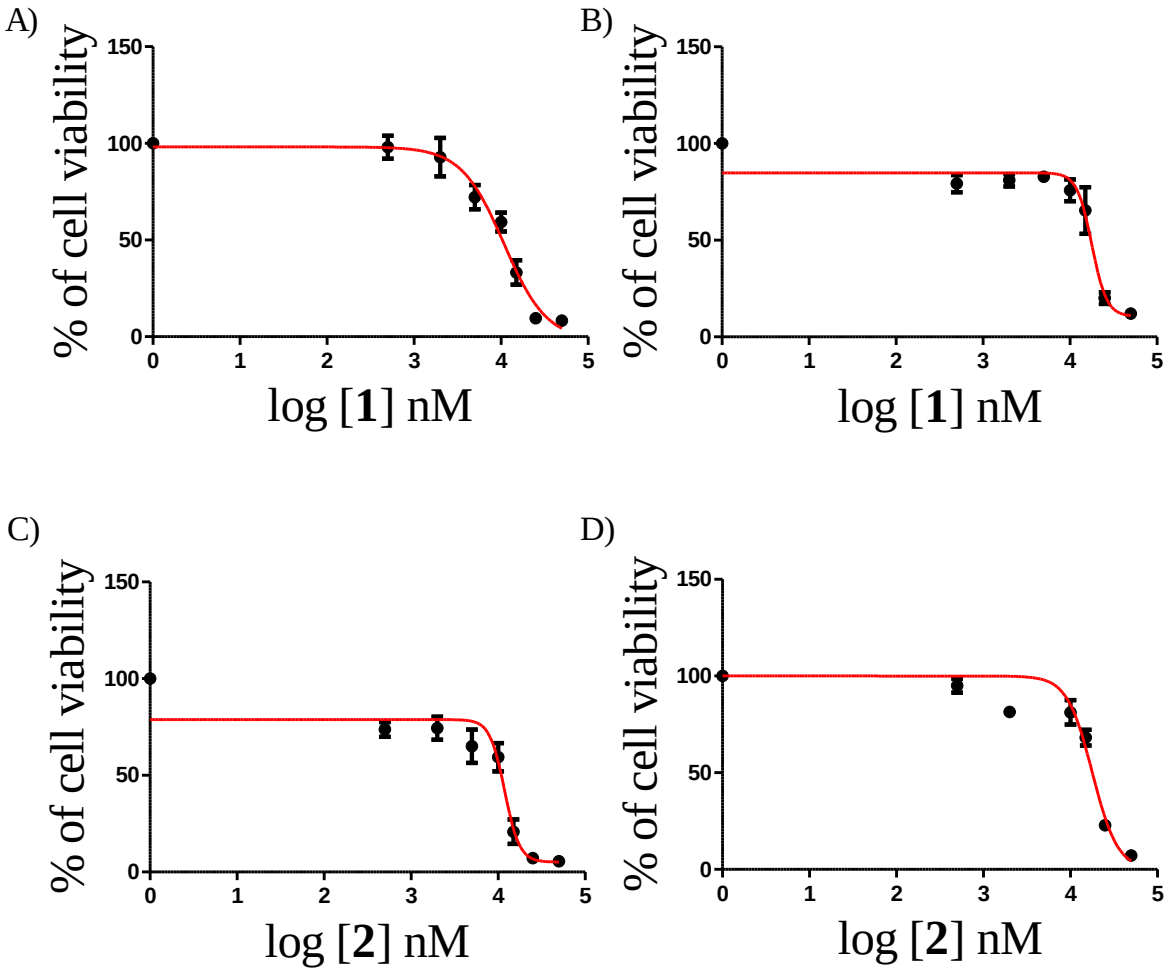

Fig. S26 Plots of cell viability (%) vs. log of concentration from MTT assays under hypoxic condition for **1** [A) MCF-7, B) A549] and **2** [C) MCF-7, D) A549] after incubation for 48 h. The plots provided are for one independent experiment out of the three independent experiments performed with each concentration.

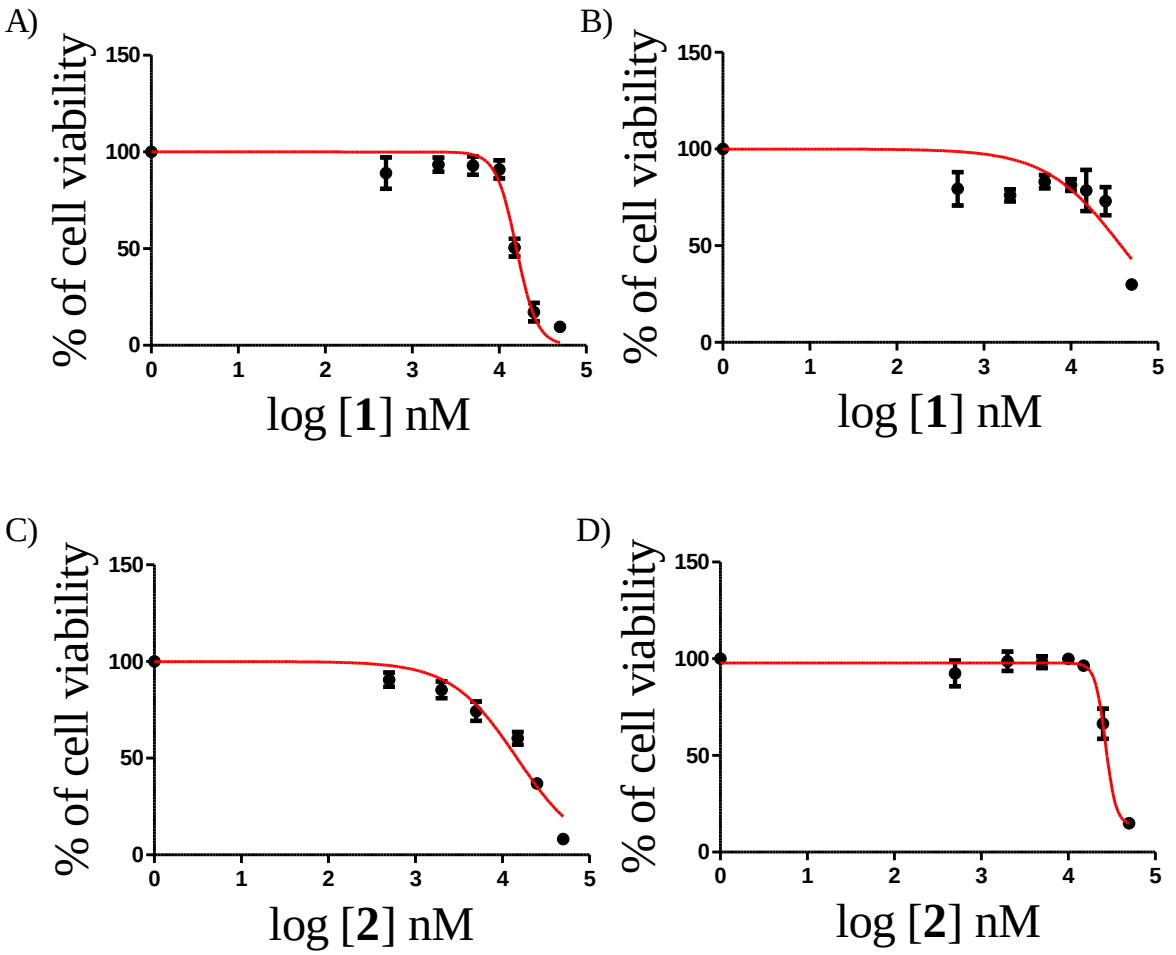

Fig. S27 Plots of cell viability (%) vs. log of concentration determined from MTT assays under hypoxic condition in presence of 1 mM L-glutathione after incubation for 48 h: for **1** A) MCF-7, B) A549 and for **2** C) MCF-7, D) A549 cell lines. The plots provided are for one independent experiment out of the three independent experiments performed with each concentration.

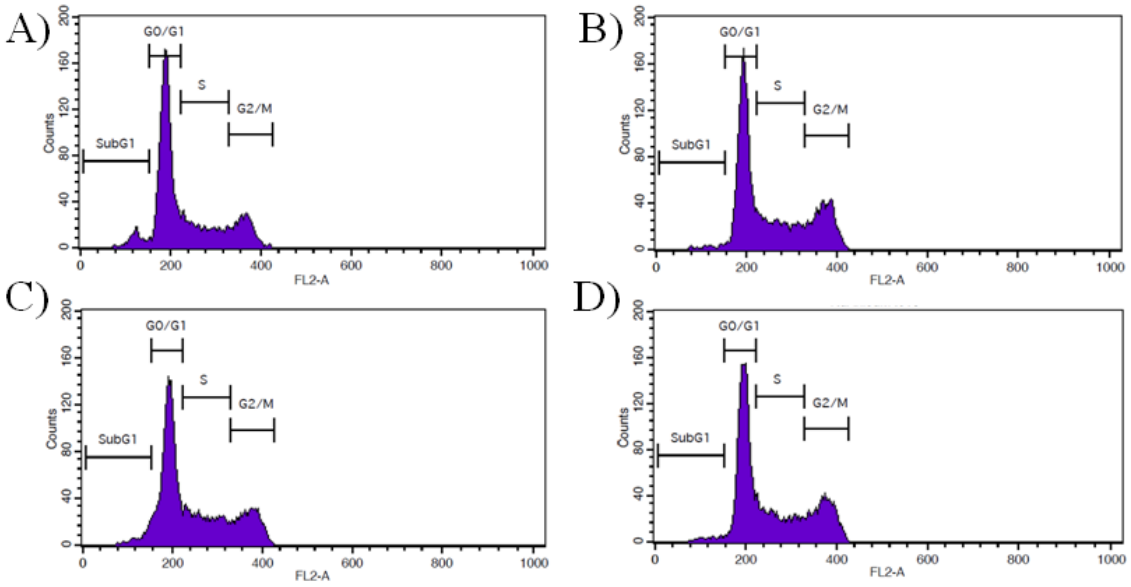

Fig. S28 Cell cycle analysis of MCF-7 cells treated with **1** for 24h. (A) DMSO control, (B) 2 μM and (C) 4 μM and D) 6 μM of **1**. The figure represents one independent experiment.

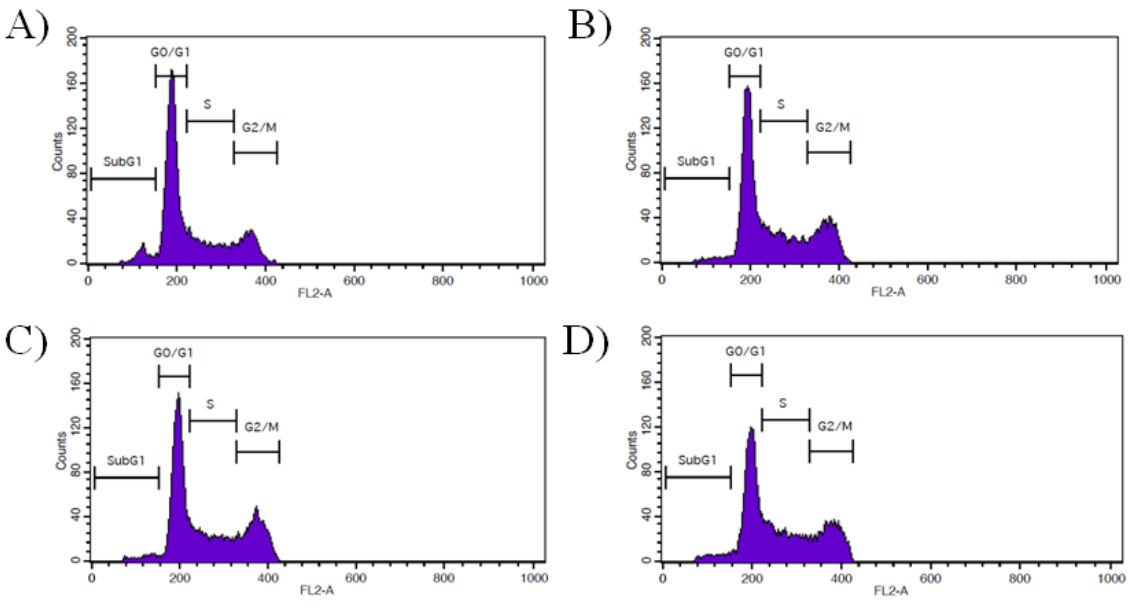

Fig. S29 Cell cycle analysis of MCF-7 cells treated with **2** for 24h. A) represents DMSO control while B), C) and D) represents 2, 4 and 6 μM of **2** treated cells. The figure represents one independent experiment.

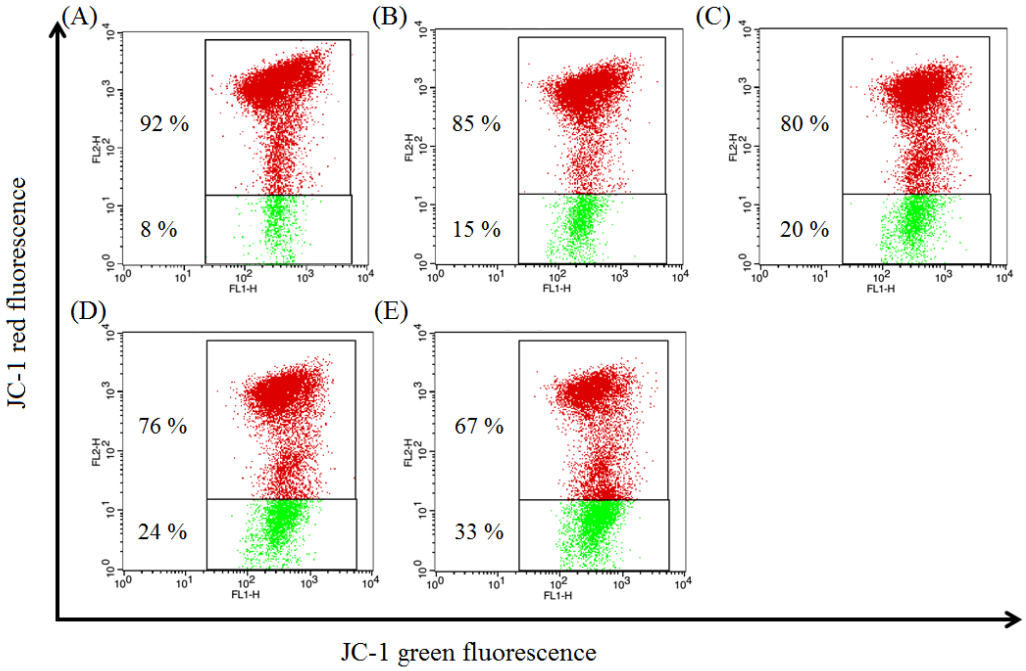

Fig. S30 FACS analysis of JC-1 stained MCF-7 cells after treatment with **1** for 48 h. JC-1was used as a probe for observing the change in mitochondrial transmembrane potential. (A) DMSO (0.2%); (B) **1** (2 μM); (C) **1** (4 μM); (D) **1** (8 μM) and (E) **1** (10 μM).

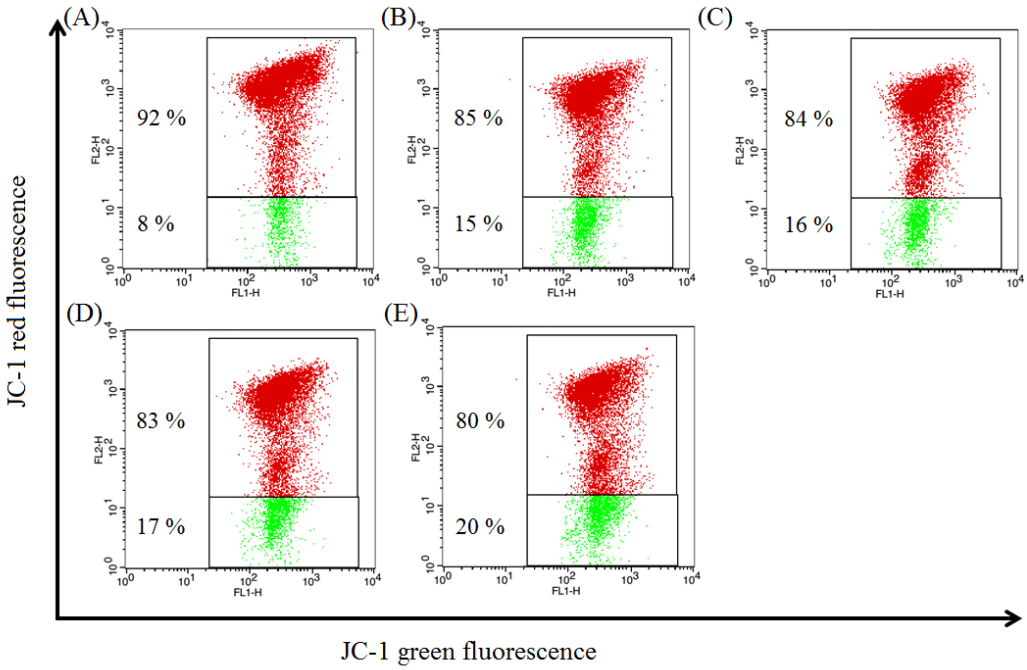

Fig. S31 FACS analysis of JC-1 stained MCF-7 cells after treatment with **2** for 48 h. JC-1was used as a probe for observing the change in mitochondrial transmembrane potential. (A) DMSO (0.2%); (B) **2** (2 μM); (C) **2** (4 μM); (D) **2** (8 μM) and (E) **2** (10 μM).

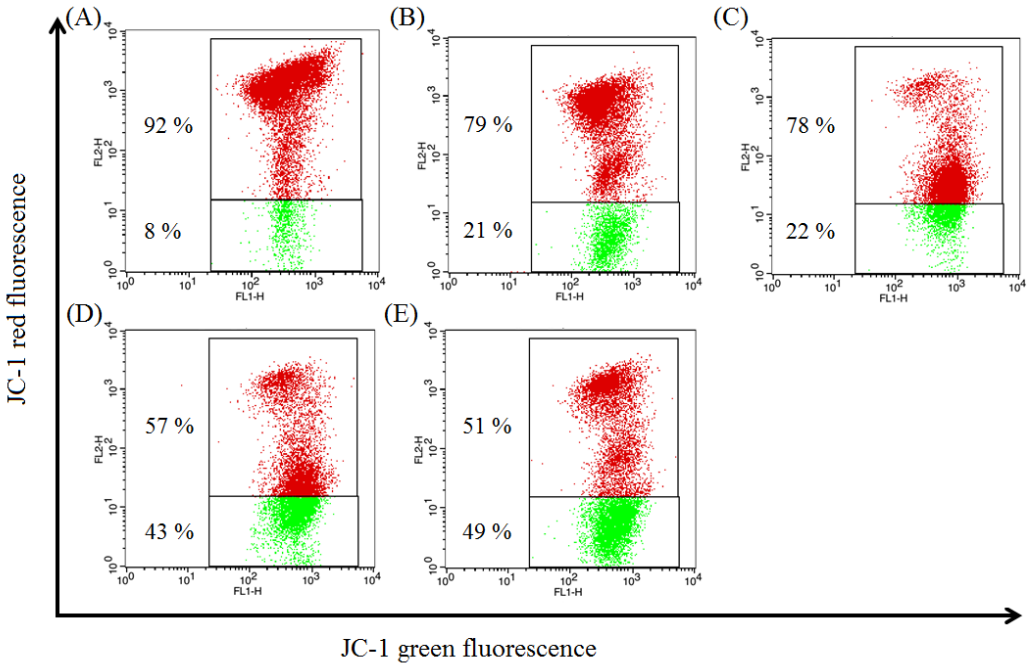

Fig. S32 FACS analysis of JC-1 stained MCF-7 cells after treatment with **3** for 48 h. JC-1was used as a probe for observing change in mitochondrial transmembrane potential. (A) DMSO (0.2%); (B) **3** (2 μM); (C) **3** (4 μM); (D) **3** (8 μM) and (E) **3** (10 μM).

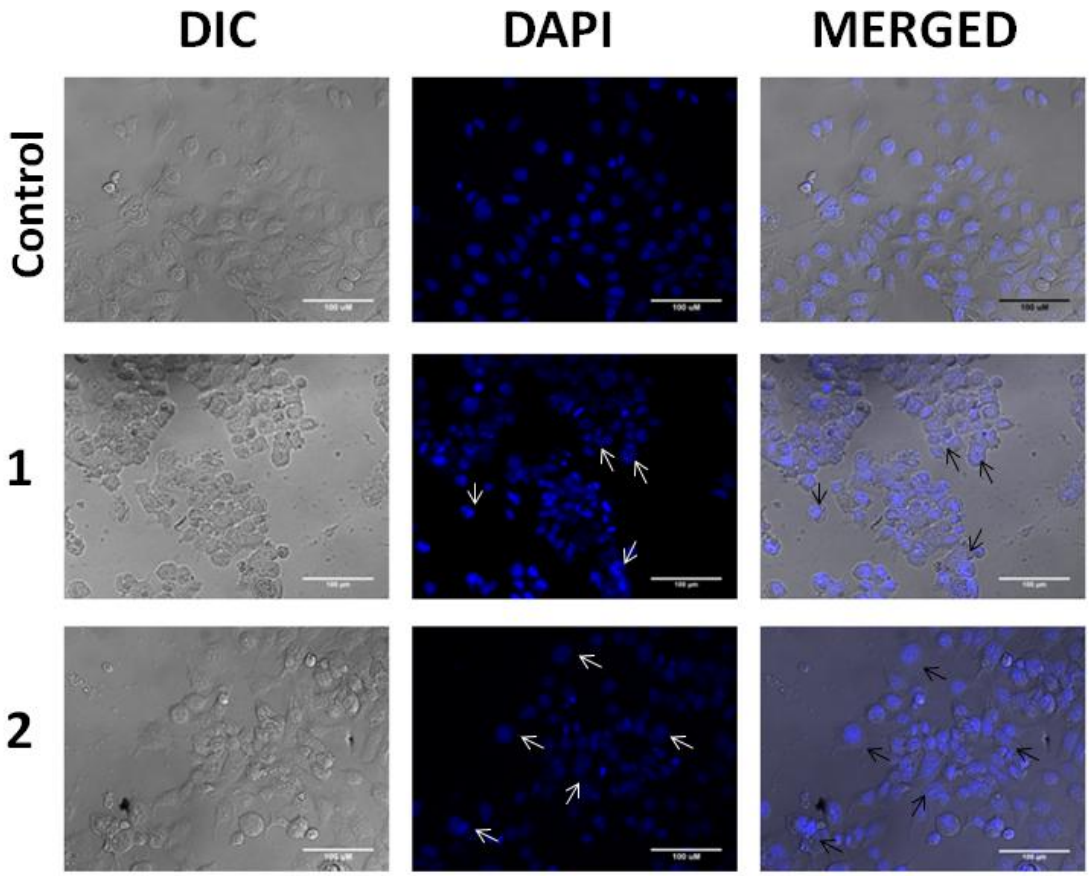

Fig. S33 Fluorescence microscopic images of MCF-7 after 24 h incubation with **1** and **2** (DAPI stained). The nuclear morphological changes in cells are indicated by arrows upon the treatment of **1** and **2** (6 μM) with respect to control (DMSO treated (< 0.2%)).

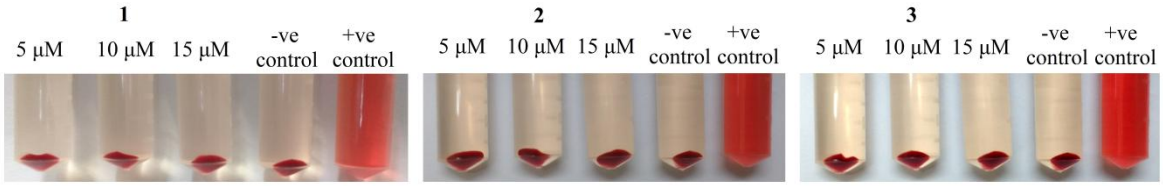

Fig. S34 Haemolysis of blood samples upon treatment with complexes **1-3**.

Table S5. Human blood compatibility test of complex **1-3** with three different concentrations in presence of +ve and –ve control.[a]

Complex	Complex concentration		
	5µM	10 µM	15 µM
1	0.45±0.3	0.5±0.3	0.98±0.5
2	0.70±0.73	1.66±0.26	1.31±0.33
3	1.31±0.26	1.91±0.49	2.57±0.28

[a]Three independent experiment were performed and average values with standard deviations are reported.

Reference

1. Purkait, K.; Karmakar, S.; Bhattacharyya, S.; Chatterjee, S.; Dey, S. K.; Mukherjee, A. A hypoxia efficient imidazole-based Ru^{II} arene anticancer agent resistant to deactivation by glutathione. *Dalton Trans.* **2015,** 44, 5969-5973.